JOURNAL OF GEOPHYSICAL RESEARCH, VOL. 95, NO. A1, PAGES 149–172, JANUARY 1, 1990

Electrostatic Lower Hybrid Waves Excited by Electromagnetic Whistler Mode Waves Scattering From Planar Magnetic-Field-Aligned Plasma Density Irregularities

T. F. BELL AND H. D. NGO

STAR Laboratory, Stanford University, Stanford, California

Recent satellite observations demonstrate that high amplitude, short wavelength (5 m $\leq \lambda \leq$ 100 m) electrostatic waves are commonly excited by electromagnetic whistler mode waves propagating in regions of the magnetosphere and topside ionosphere where small-scale magnetic-field-aligned plasma density irregularities are thought to exist. A new theoretical model of this phenomenon is presented, based upon passive linear scattering in a cold magnetoplasma. In this model the electrostatic waves are excited by linear mode coupling as the incident electromagnetic whistler mode waves scatter from the magnetic-field-aligned plasma density irregularities. The excited short wavelength waves are quasi-electrostatic whistler mode waves, a type of lower hybrid wave, whose wave normal lies near the whistler mode resonance cone where the wave refractive index becomes very large. For simplicity the case of planar irregularities is considered in which the electron density varies in only a single direction, roughly perpendicular to $\mathbf{B}_0$, the Earth's magnetic field. The amplitude of the excited electrostatic lower hybrid waves is calculated for a wide range of values of input electromagnetic wave frequency, wave normal direction, electron plasma frequency, gyrofrequency, ion composition, and irregularity scale and density enhancement. Results indicate that high amplitude lower hybrid waves can be excited over a wide range of parameters for irregularity density enhancements as low as 5% whenever the scale of the irregularity is of the same order as the lower hybrid wavelength. It is shown that lower hybrid waves can be excited only when the planar irregularities are aligned with $\mathbf{B}_0$ within a small angle $2\chi_c$, where χ_c is equal to the complement of the resonance cone half-angle. For the frequencies and L shells considered, $\chi_c \leq 8^\circ$. Predictions of the theory are shown to be consistent with satellite data. A VLF "radar" method is demonstrated whereby the lower hybrid wave excitation phenomenon can be used as a diagnostic tool to determine the small scale irregularity structure of the medium. The effective damping of the input electromagnetic wave due to the excitation of the lower hybrid waves is also considered. It is found that this form of damping may be a dominant factor for whistler mode waves throughout large regions of the magnetosphere.

1. INTRODUCTION

Recent data from the ISEE 1, DE 1, ISIS 1, ISIS 2, and Aureol 3 satellites [*Bell et al.*, 1983; *Titova et al.*, 1984; *Tanaka et al.*, 1984; *Inan and Bell*, 1985; *Bell and Ngo*, 1988] suggest that high amplitude electrostatic waves are commonly excited by electromagnetic VLF whistler mode waves propagating through regions of the ionosphere and magnetosphere where magnetic-field-aligned plasma density irregularities exist. These waves cut off at the lower hybrid resonance frequency and are a type of lower hybrid wave.

Since the excited lower hybrid waves can interact with energetic particles, the phenomenon may be an important factor in wave-particle interactions in the ionosphere and magnetosphere and also may be involved in the creation and maintenance of systems of small scale magnetic-field-aligned plasma density irregularities [*Bell and Ngo*, 1988].

A number of possible mechanisms for producing the lower hybrid waves have been discussed in the literature [*Bell et al.*, 1983; *Titova et al.*, 1984; *Ngo and Bell*, 1985; *Bell and Ngo*, 1988; *Groves et al.*, 1988]. It is the purpose of the present paper to focus upon one of the simplest generation mechanisms proposed to date, namely, that the lower hybrid waves are excited as the electromagnetic whistler mode waves scatter from magnetic-field-aligned plasma density irregularities in the ionosphere and magnetosphere [*Bell et al.*, 1983; *Ngo and Bell*, 1985; *Bell and Ngo*, 1988]. As we show below, the lower hybrid wave excitation occurs at the boundaries of the irregularity as a natural consequence of the application of Maxwell's equations in a cold passive magnetoplasma. It is therefore not necessary to invoke plasma instabilities or parametric interactions to explain the observed features of the phenomenon.

It is well known that a cold uniform magnetoplasma is doubly refractive, i.e., there are four normal modes of wave propagation for any given direction of propagation. The refractive indices and polarization of the four normal modes are given, for example, in *Stix* [1962] and in *Budden* [1985]. As a result of this situation, a single propagating normal mode can excite as many as four normal modes when it scatters from a discontinuity in the plasma. In particular, for the case of a whistler mode wave scattering from a magnetic-field-aligned plasma density irregularity, two of the four excited normal modes can be quasi-electrostatic lower hybrid waves of short wavelength.

Figure 1 illustrates how this situation can come about. It is assumed that the magnetoplasma consists of two semi-infinite uniform media, region I and region II. The cold plasma density, N, is assumed to differ slightly in the two regions, so that $N_1 \neq N_2$. In each region we plot (not to scale) the whistler mode refractive index surface $n(\theta)$ as a function of the angle θ between the vector $\mathbf{n}$ and the z axis, which lies parallel to the ambient magnetic field direction. It is assumed that the wave frequency is less than roughly one-half the electron gyrofrequency f_{He}, but higher than the local lower hybrid resonance frequency f_{LHR} so that

Paper number 89JA01200.
0148-0227/90/89JA-01200$05.00

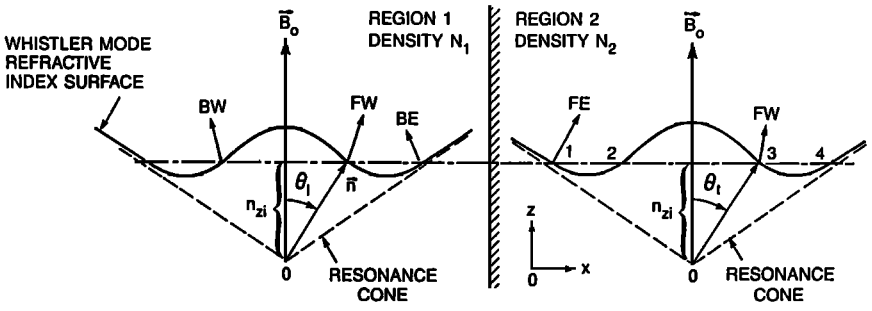

Fig. 1. Schematic representation illustrating how quasi-electrostatic, lower hybrid waves are stimulated by electromagnetic whistler mode waves as a natural byproduct of reflection and transmission at a magnetic-field-aligned plasma density discontinuity.

the refractive index surface approaches infinity along the resonance cone direction. It is also assumed that a whistler mode wave of wave normal angle θ_i propagates toward the boundary from region I, and, for simplicity, that the wave normal lies in the x-z plane.

For the incident wave, the component of the refractive index parallel to the boundary has the value $n_{zi} = n(\theta_i)\cos\theta_i$, and by Snell's law all transmitted and reflected waves must have this same value for n_z. In each region the line $n_z = n_{zi}$ cuts the whistler mode refractive index surface at four points. The wave normal angles associated with these points define the four normal modes which are the solutions to Maxwell's equations in each region. Thus all four possible solutions in each region are propagating whistler mode waves. However in each region two of the possible solutions for $n(\theta)$ lie near the resonance cone where $n \to \infty$. These solutions on the resonance cone represent quasi-electrostatic whistler mode waves of relatively short wavelength. The quasi-electrostatic waves are a type of lower hybrid wave and possess the property that their electric vector E is nearly parallel to their wave vector k, whereas for the electromagnetic whistler mode waves k is roughly perpendicular to E.

As shown in section 2, the four possible values of the transverse component of the refractive index, $n_\perp$, are given for each region by the relation

$$n_\perp^4 - 2\beta_1 n_\perp^2 + \beta_2 = 0 \tag{1}$$

where

$$\beta_1 \equiv [P + RL/S - n_{zi}^2(1 + P/S)]/2$$
$$\beta_2 \equiv (n_{zi}^4 - 2Sn_{zi}^2 + RL)P/S$$
$$n_\perp^2 \equiv n_x^2 + n_y^2$$

and where the plasma coefficients R, L, S, and P are defined in *Stix* [1962, chapter I], and are assumed to be evaluated separately in each region. Quasi-electrostatic lower hybrid solutions for (1) occur when $f_{LHR} \leq f \ll f_{He}$, in which case S is small.

For the present case in which the wave normal lies in the x-z plane, we have $n_y = 0$ and the four solutions to (1) can be expressed in the form

$$n_x = \pm\left(\beta_1 \pm \sqrt{\beta_1^2 - \beta_2}\right)^{1/2} \tag{2}$$

where each of the four possible combinations of signs defines a separate value of n_x. The two possible quasi-electrostatic waves in a given region are defined by the choice of the plus sign within the bracket in (2).

For input wave frequencies in the range $f_{LHR} \leq f \ll f_{He}$, where f_{He} is the electron gyrofrequency, the values of n_x for the two possible quasi-electrostatic lower hybrid waves are given by the approximate relation

$$n_x^{ES} = \pm f_{He} n_{zi}(f^2 - f_{LHR}^2)^{-1/2}$$
$$\cong \pm f_{0e} f_{He}^{1/2} f^{-1/2}(f^2 - f_{LHR}^2)^{-1/2}(\cos\theta_i)^{1/2} \tag{3}$$

where f_{0e} is the electron plasma frequency. Under the conditions shown in the figure, not all possible solutions are allowed in each region since we assume a single input wave from region I and only outgoing waves in region II. Consequently, the initial electromagnetic input wave will excite a reflected electromagnetic wave and a "reflected" lower hybrid wave in region I and a transmitted electromagnetic wave and a "transmitted" lower hybrid wave in region II.

It is clear that if the input wave encounters multiple surfaces of discontinuity as it propagates across $\mathbf{B}_0$ the space between these surfaces will contain stimulated lower hybrid waves with wave normals both in the positive and negative x direction. In this case the lower hybrid waves would be observed on a moving spacecraft with both positive and negative Doppler shifts.

Figures 2 and 3 show the main details of our model of the stimulation process. Figure 2 shows the case of a single scattering event. The incident electromagnetic whistler mode wave encounters a single planar magnetic-field-aligned plasma density irregularity whose width transverse to $\mathbf{B}_0$ is much smaller than the wavelength of the incident wave. Although most of the incident whistler mode wave energy is transmitted through the irregularity, during the scattering process two quasi-electrostatic lower hybrid waves are excited which propagate on opposite sides of the irregularity at a small angle δ with respect to the direction of the Earth's magnetic field $\mathbf{B}_0$. Lower hybrid waves are also excited within the irregularity. The wave vector $\mathbf{k}_{ES}$ of each lower hybrid wave is nearly perpendicular to the group velocity vector $\mathbf{V}_{GES}$ of the wave and the propagation angle δ is approximately equal to the complement of the whistler mode resonance cone half angle ψ_r defined by the relation $\psi_r = \tan^{-1}(-P/S)^{1/2}$. In general, δ is quite small ($\leq 8°$) for the cases we will consider. It is shown much larger in the figure merely for illustrative purposes.

Figure 3 shows the general case where a number of planar magnetic-field-aligned plasma density irregularities are

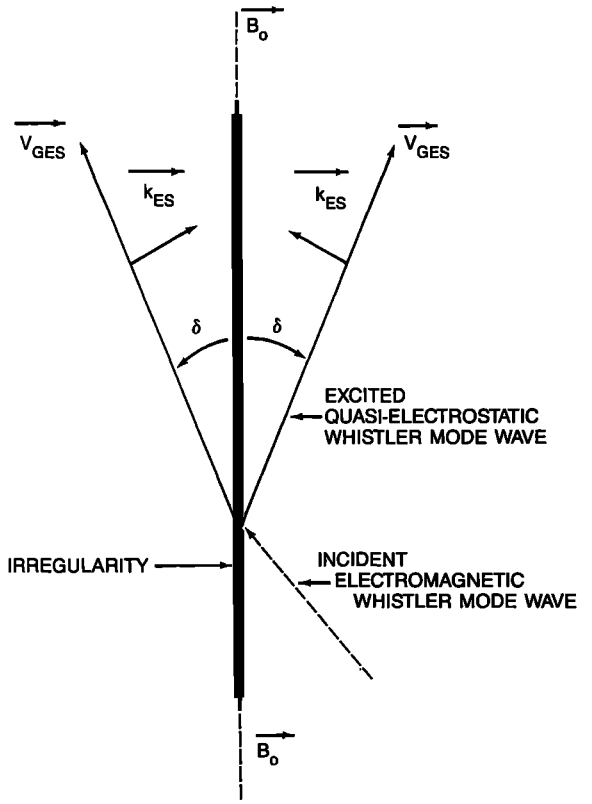

Fig. 2. Schematic representation showing the case of an incident electromagnetic whistler mode wave scattering from a single planar magnetic-field-aligned plasma density irregularity. Quasi-electrostatic, lower hybrid waves are excited at both boundaries of the irregularity and propagate at an angle δ with respect to $\mathbf{B}_0$.

involved in the scattering process. Once again we have exaggerated the scale of δ for illustrative purposes. It is assumed that the irregularities occupy a length $\Delta\ell$ along $\mathbf{B}_0$ and are located roughly at a distance R from the observing spacecraft. Although the incident electromagnetic whistler mode waves will excite lower hybrid waves each time they encounter an irregularity, only those lower hybrid waves whose ray path intersects the spacecraft will be observed. If neither the ambient magnetic field nor the ambient plasma density varies significantly over the distances R and $\Delta\ell$, the situation is simplified and the necessary condition for observability is just that the group velocity vector $\mathbf{V}_{GES}$ of an excited lower hybrid wave must lie on the surface of the cone of half angle δ which is centered on the magnetic field line through the spacecraft position and whose vertex is centered on the spacecraft. The figure shows three lower hybrid waves whose $\mathbf{V}_{GES}$ lies on this cone and which will propagate to the spacecraft. These three waves are excited at different distances from the spacecraft and illustrate the fact that at any one time the waves received may have originated at distances over the entire range $\Delta\ell$. Since the plasma parameters f_{He} and f_{0e} generally vary over $\Delta\ell$, the lower hybrid waves received at the spacecraft will possess a range of values of wave number Δk^{ES}, where using (3) we can write

$$\Delta k^{ES} \cong \tfrac{1}{2} k^{ES} (N_0 B_0)^{-1} \frac{d(N_0 B_0)}{dz} \Delta\ell \qquad (4)$$

where N_0 is the local background plasma density and B_0 is the local magnitude of the Earth's magnetic field. In the topside ionosphere (300–600 km) where N_0 changes rapidly with altitude, the spread of k^{ES} values can be as large as 50% for $\Delta\ell \sim 100$ km. For higher altitudes where N_0 varies more slowly, Δk^{ES} will depend primarily upon the variation of the Earth's magnetic field over the distance $\Delta\ell$.

As we will demonstrate in section 4, the group velocity of the excited lower hybrid waves is much less than that of the incident electromagnetic waves. Thus the lower hybrid waves will arrive at the spacecraft with a significant time delay with respect to the input electromagnetic waves. Furthermore, they will be observed with a significant Doppler shift because of their short wavelength. The time delay and Doppler shift information can be used together to determine the range R from the spacecraft to the excitation point of the lower hybrid waves [*Bell et al.*, 1983]. Experimental observations at high altitudes [*Bell and Ngo*, 1988] indicate that the range R can vary from zero to thousands of kilometers, and that the irregularities at times may extend between hemispheres.

Although the foregoing model suggests how lower hybrid waves can be stimulated and observed on spacecraft, it does not determine the amplitudes of the stimulated waves. For these answers we need to solve the wave equation.

2. Wave Equation in a Cold Magnetoplasma

Geometrical Features

Figure 4 shows the geometry of our study. It is assumed that the cold magnetoplasma is homogeneous everywhere except for the limited region of space, $x_1 \leq x \leq x_M$, within which the density of the cold plasma $N(x)$ is assumed to vary as a function of x alone. Although it can be expected that $N(x)$ is generally a continuous function of x for real plasmas, we can approximated the function $N(x)$ by a series of slabs of constant density N_m whose thickness Δ_m is small compared to the width of the region $|x_M - x_1|$ in which $N(x)$ varies. The approximation scheme is shown in Figure 5*a*. If the number of slabs is sufficiently large, $N(x)$ can be approximated to as high a degree as desired by the step function.

It is assumed that, in general, the ambient magnetic field $\mathbf{B}_0$ is not directed parallel to the planar faces of the constant density slabs but instead is tilted at an angle χ with respect to the planar faces. Without loss of generality the Cartesian coordinate system can be rotated about the x axis so that $\mathbf{B}_0$ lies in the x–z plane, as shown in Figure 4. The wave normal vector $\mathbf{k}$ of the wave incident on the planar irregularity has a direction described by a polar angle θ with respect to the z axis and an azimuthal angle ϕ, measured in the x–y plane in a clockwise direction from the x axis. Although shown with finite cross section in Figure 4, each of the planar slabs is assumed to extend toward infinity parallel to the z and y axes.

Although the theory we use below is valid for all values of tilt angle χ, we are concerned mainly with cases in which the irregularities are aligned within a few degrees of $\mathbf{B}_0$. As we show below, important changes in our model can occur at small values of χ; however most major features are evident in the simpler case $\chi = 0$, for which the irregularities are exactly aligned with $\mathbf{B}_0$. Consequently it is instructive to first consider solutions to the wave equation for the case $\chi = 0$.

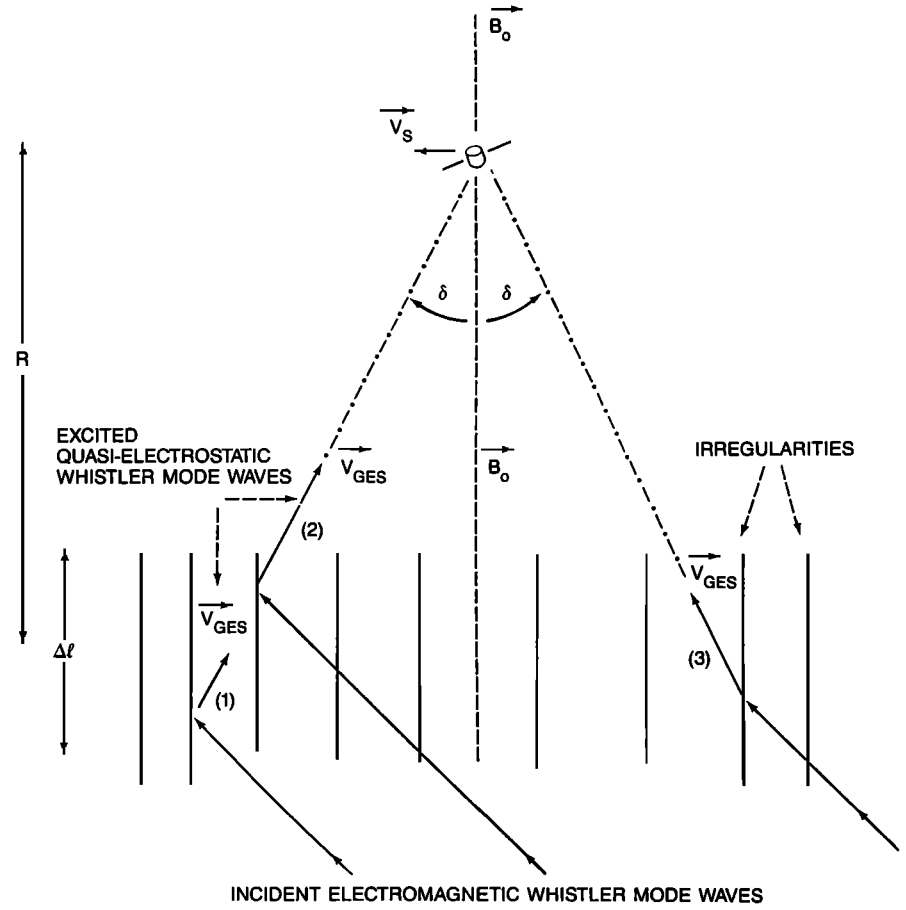

Fig. 3. Schematic representation showing the general case of an incident electromagnetic whistler mode wave scattering from a number of magnetic-field-aligned plasma density irregularities. Lower hybrid waves are excited along the length of each irregularity but only waves propagating toward the spacecraft position are shown.

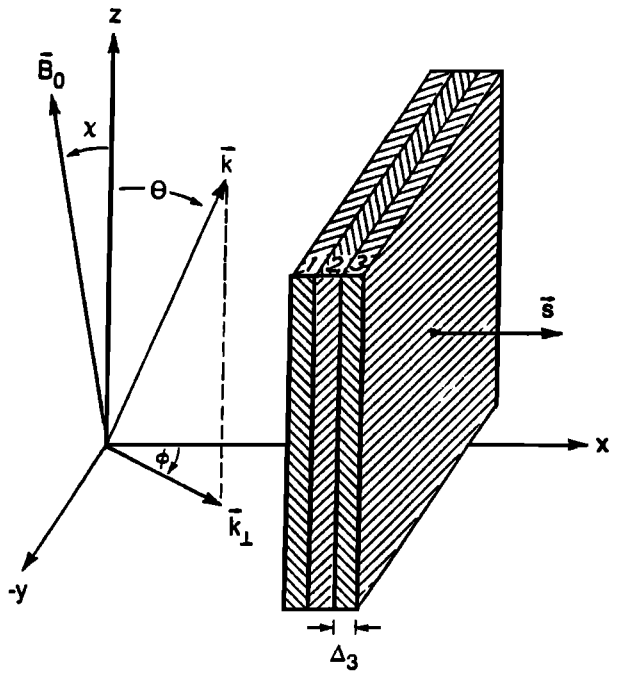

Fig. 4. General geometry of study where the x axis is normal to the irregularity surface, $\mathbf{B}_0$ lies in the x-z plane, and the incident whistler mode wave normal vector k can have an arbitrary direction.

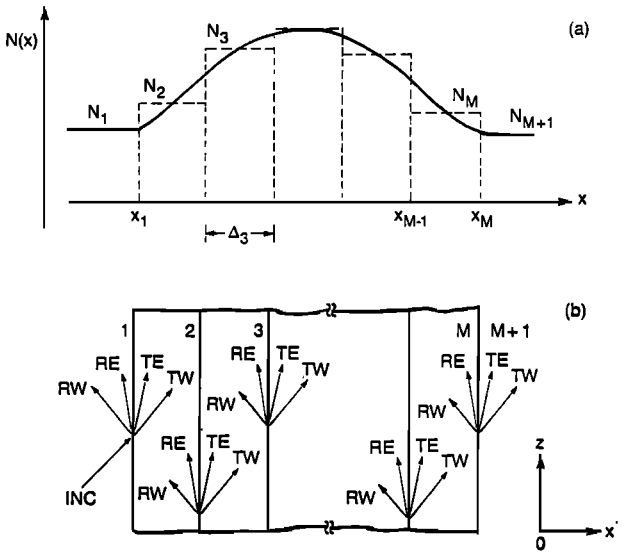

Fig. 5. Method of solution for the case of one-dimensional variable plasma density profile $N(x)$. (a) Approximation by a series of $M - 1$ slabs of constant density. (b) Full wave solution applied to each slab. INC, incident whistler mode wave. RE, leftward propagating stimulated lower hybrid wave. RW, reflected electromagnetic whistler mode wave. TE, rightward propagating stimulated lower hybrid wave. TW, transmitted electromagnetic whistler mode wave.

Irregularities Exactly Aligned With $\mathbf{B}_0$

From Maxwell's equations for time harmonic fields $e^{i\omega t}$ we have

$$\nabla \times \mathbf{E} = -\frac{\partial \mathbf{B}}{\partial t} = -i\omega \mathbf{B} \tag{5}$$

$$\nabla \times \mathbf{B} = \mu_0 \varepsilon_0 \frac{\partial}{\partial t}(\underline{\mathbf{K}} \cdot \mathbf{E}) = \frac{i\omega}{c^2}\underline{\mathbf{K}} \cdot \mathbf{E} \tag{6}$$

where the dielectric tensor $\underline{\mathbf{K}}$ appears under our convention of time dependence in the form

$$\underline{\mathbf{K}} \cdot \mathbf{E} = \begin{pmatrix} S & iD & 0 \\ -iD & S & 0 \\ 0 & 0 & P \end{pmatrix} \begin{pmatrix} E_x \\ E_y \\ E_z \end{pmatrix} \tag{7}$$

Note that $\mathbf{K}$ is invariant with respect to rotation about the z axis and is the complex conjugate to that defined by *Stix* [1962]. The various parameters in $\mathbf{K}$ are defined exactly as in *Stix* [1962] and are repeated here in MKS units for convenient reference:

$$S \equiv (R+L)/2 \tag{8a}$$

$$D \equiv (R-L)/2 \tag{8b}$$

$$R \equiv 1 - \sum_k \frac{\omega_{0k}^2}{\omega^2}\left(\frac{\omega}{\omega + \epsilon_k \omega_{Hk}}\right) \tag{8c}$$

$$L \equiv 1 - \sum_k \frac{\omega_{0k}^2}{\omega^2}\left(\frac{\omega}{\omega - \epsilon_k \omega_{Hk}}\right) \tag{8d}$$

$$P \equiv 1 - \sum_k \frac{\omega_{0k}^2}{\omega^2} \tag{8e}$$

$$\omega_{0k}^2 \equiv \frac{N_k Z_k^2 e^2}{m_k \varepsilon_0} \tag{8f}$$

$$\omega_{Hk} \equiv \left|\frac{Z_k e B_0}{m_k}\right| \tag{8g}$$

Here, N_k is the number density of particles of species k with charge magnitude $Z_k e$. The sign of charge, ± 1, is given by ϵ_k.

It is instructive to first consider the simple case, shown in Figure 1, in which the plasma consists of only two distinct regions, both of which are homogeneous. In region I ($-\infty < x < 0$), $N(x) = N_1$, and in region II ($0 < x < \infty$), $N(x) = N_2$. At the boundary between the two regions, $x = 0$, the density changes abruptly from N_1 to N_2.

Since both regions I and II are homogeneous, general solutions to the wave equation in each region for components of $\mathbf{E}$ or $\mathbf{B}$ will consist of plane waves of the form $e^{i(\omega t - \mathbf{k}\cdot\mathbf{r})}$, where $\mathbf{k} = \omega \mathbf{n}/c$, and where the magnitude of the refractive index, n, is one of the four solutions to the well known dispersion relation [*Stix*, 1962]

$$a_1 n^4 - a_2 n^2 + a_3 = 0 \tag{9}$$

where

$$a_1 = S\sin^2\theta + P\cos^2\theta$$

$$a_2 = RL\sin^2\theta + PS(1+\cos^2\theta)$$

$$a_3 = PRL$$

By Snell's law the values of n_y and n_z must be conserved across the boundary between regions I and II, i.e., $n_y = n_{yi}$ and $n_z = n_{zi}$. Thus only the value of n_x remains to be determined for each plane wave solution. One simple method is to replace in (9) each occurence of $n\cos\theta$ by n_z and $n\sin\theta$ by $n_\perp$ where $n_\perp$ is defined in (1). When this is done, we obtain an equation as given in (1) and a set of four solutions exactly the same as (2) with n_x replaced by $n_\perp$. Thus we can write the general solution for each cartesian component of the wave electric and magnetic fields in the form

$$\psi(x,y,z) = \left[Ae^{-ik_{x1}x} + Be^{ik_{x1}x} + Ce^{-ik_{x2}x} + De^{ik_{x2}x}\right]e^{-i(k_z z + k_y y)} \tag{10}$$

where

$$k_{x\nu} = \frac{\omega}{c}\sqrt{n_{\perp,\nu}^2 - n_y^2} \qquad \nu = 1,2$$

$$n_{\perp,1} = \left(\beta_1 - \sqrt{\beta_1^2 - \beta_2}\right)^{1/2}$$

$$n_{\perp,2} = \left(\beta_1 + \sqrt{\beta_1^2 - \beta_2}\right)^{1/2}$$

and where β_1 and β_2 are defined in (1) and where all the constant coefficients (A, B, C, and D) associated with each Cartesian component of the field can be expressed in terms of the four similar coefficients associated with the other components through relations (5) and (6)

In order to relate the solutions on either side of the planar boundary we can make use of the boundary conditions which require that the tangential components of $\mathbf{E}$ and $\mathbf{H}$ be continuous at $x = 0$, i.e.,

$$E_j^{total}\Big|_{x=0-} = E_j^{total}\Big|_{x=0+} \qquad j = y, z \tag{11}$$

$$H_j^{total}\Big|_{x=0-} = H_j^{total}\Big|_{x=0+}$$

A second boundary condition concerns the form of the solutions in the two regions at distances far from the planar boundary at $x = 0$. If we assume that the incident electromagnetic whistler mode wave propagates toward this boundary from the region $x < 0$, then the general solution in this region must consist of the incident wave, propagating in the positive x direction, plus two waves propagating in the negative x direction. One of these backward propagating waves is an electromagnetic whistler mode wave, and one is a quasi-electrostatic whistler mode wave of lower hybrid type. The general solution in the second region, $x > 0$, must consist only of waves propagating away from the boundary toward the positive x direction. Thus for our problem the general solutions in the two regions have the form

$$\psi(x<0,y,z) = \left[A_1 e^{-ik_{x1}x} + B_1 e^{ik_{x1}x} + C_1 e^{-ik_{x2}x}\right]e^{-i(k_{zi}z + k_{yi}y)} \tag{12a}$$

$$\psi(x>0,y,z) = \left[A_2 e^{-ik'_{x1}x} + D_2 e^{ik'_{x2}x}\right] \times e^{-i(k_{zi}z + k_{yi}y)} \tag{12b}$$

where the prime indicates that the concerned quantity is evaluated in the second medium. The boundary conditions of (11) insure that the Poynting flux across the boundary $x = 0$ is continuous. The direction of propagation of each plane wave component can be determined by evaluating the real part of the complex Poynting flux, $\mathbf{P} = \frac{1}{2}\mathbf{E} \times \mathbf{H}^*$, for each component. This evaluation shows that for the electromagnetic whistler mode waves with $k_x = k_{x1}$ the phase velocity and the group velocity in the x direction have the same sign, while for the lower hybrid waves with $k_x = k_{x2}$,

the phase velocity and group velocity along x have opposite signs. This feature can be seen in Figure 1. Since the group velocity vector is normal to the refractive index surface and since this surface is asymptotic to the resonance cone for large values of n_x, it is clear that $\mathrm{sgn}(n_x) = -\mathrm{sgn}(V_{Gx})$. Thus the spatial phase factors of the stimulated electromagnetic and electrostatic components have opposite signs in (12).

Using the general solution of (12), we apply (11) to arrive at the following relations for the E_z and E_y components:

$$E_z^{IWM} + E_z^{RWM} + E_z^{RES} = E_z^{TWM} + E_z^{TES} \quad (13a)$$

$$E_y^{IWM} + E_y^{RWM} + E_y^{RES} = E_y^{TWM} + E_y^{TES} \quad (13b)$$

where E_j^{IWM} is the amplitude of the incident electromagnetic (EM) whistler mode wave in region I, E_j^{RWM} is the amplitude of the reflected EM whistler mode wave in region I, E_j^{RES} is the amplitude of the lower hybrid wave excited in region I, E_j^{TWM} is the amplitude of the transmitted EM whistler mode wave in region II, E_j^{TES} is the amplitude of the lower hybrid wave excited in region II. Relations similar to (13a) and (13b) apply to the magnetic field amplitudes $B_{y,z}$ of the individual waves. Using (5) these may be written in terms of the electric field amplitudes:

$$\begin{aligned} &k_{x1}E_y^{IWM} - k_{x1}E_y^{RWM} + k_{x2}E_y^{RES} \\ &- k_y\left[E_x^{IWM} + E_x^{RWM} + E_x^{RES}\right] \\ &= k'_{x1}E_y^{TWM} - k'_{x2}E_y^{TES} - k_y\left[E_x^{TWM} + E_x^{TES}\right] \end{aligned} \quad (13c)$$

$$\begin{aligned} &k_z\left[E_x^{IWM} + E_x^{RWM} + E_x^{RES}\right] \\ &- k_{x1}E_z^{IWM} + k_{x1}E_z^{RWM} - k_{x2}E_z^{RES} \\ &= k_z\left[E_x^{TWM} + E_x^{TES}\right] - k'_{x1}E_z^{TWM} + k'_{x2}E_z^{TES} \end{aligned} \quad (13d)$$

Equations (13) represent a set of four simultaneous equation in 12 unknowns. However the number of unknowns may be reduced to 4 by making use of the polarization relationships between the electric field components of each individual plane wave that must apply if that wave is to represent a characteristic solution of (5) and (6). The polarization ratios have the values

$$\begin{aligned} \rho_y^m &\equiv E_y^m/E_x^m = \frac{iD(n_\perp^2 - P) + n_x n_y(n^2 - P)}{(n^2 - S)(n_x^2 - P) + n_y^2(P - S)} \\ \rho_z^m &\equiv E_z^m/E_x^m = \frac{n_x n_z(n^2 - S) + iDn_y n_z}{(n^2 - S)(n_x^2 - P) + n_y^2(P - S)} \end{aligned} \quad (14)$$

where ρ_y^m is the polarization ratio for the mth plane wave component (e.g., $\rho_y^{RWM} \equiv E_y^{RWM}/E_x^{RWM}$), where D, S, and P have values appropriate to the region in which the plane wave component is located, and where n_x is given implicitly by (10) and has the value appropriate to the plane wave component considered. With the use of (14) we can express the system (13) in the form

$$\underline{\mathbf{A}}\,\mathbf{E}_x = \mathbf{C} \quad (15)$$

where $\underline{\mathbf{A}}$ is a 4×4 matrix, $\mathbf{E}_x$ is a column vector consisting of the four unknown wave amplitudes, $E_x^{RWM}, E_x^{RES}, E_x^{TWM}$, and E_x^{TES}, and $\mathbf{C}$ is a column vector consisting of the four known quantities concerning the incident electromagnetic whistler mode wave. Since in general, the matrix $\underline{\mathbf{A}}$ is nonsingular, the solution to (15) is straightforward. Once the E_x^m have been found in terms of the incident wave amplitude, the quantities $E_{y,z}^m$ can be found through the polarization relations (14).

If the density irregularity is distributed over a width W, we can approximate the actual distribution by a series of constant density slabs as shown in Figure 5a. If the number of slabs is sufficiently large, the approximation approaches the exact solution. The problem becomes complicated due to multiple reflection and transmission in the presence of multiple boundaries. However, it can be attacked efficiently since there exist only four normal modes in every slab which correspond to four waves with different transverse wave numbers, k_x. As indicated schematically in Figure 5b, these four waves must be retained for each slab in the full solution, except for the two backward traveling waves in the last medium ($x > W$) and the second forward traveling wave in the first medium ($x < 0$). Imposing the boundary conditions at each boundary between slabs gives rise to a system of $4M$ algebraic equations in $4M$ unknowns where M is the number of planar boundaries. This problem can be cast into a matrix equation of the form $\underline{\mathbf{A}}\,\mathbf{E}_x = \mathbf{C}$, where $\underline{\mathbf{A}}$ is a $4M$ by $4M$ matrix. Fortunately, the matrix $\mathbf{A}$ has only $32M-12$ nonzero entries for $M \geq 2$. This is a considerable reduction in complexity as opposed to $16M^2$ nonzero entries of a full nonzero matrix. Efficient algorithms have been developed to handle successfully this particular matrix equation for up to thousands of slabs. In principle, this large matrix equation can be solved numerically to obtain E_x in every slab. The other components of $\mathbf{E}$ and $\mathbf{B}$ can then be determined as in the single boundary case by using the polarization conditions.

Irregularities Tilted With Respect to $\mathbf{B}_0$

Thus far we have considered the case in which the boundary of the planar irregularities was parallel to the ambient magnetic field $\mathbf{B}_0$. To treat the more general situation we assume that the planar boundary is tilted at an angle χ with respect to the ambient magnetic field as shown in Figure 4. Physically, we expect that the lower hybrid waves excited by the incident electromagnetic whistler mode wave will differ in character when $|\chi|$ exceeds the critical value χ_c where $\chi_c \equiv \pi/2 - \psi_r$, and where ψ_r is the resonance cone half angle. To illustrate this situation we sketch (not to scale) in Figure 6 the real part of the whistler mode refractive index surface for the entire range of wave normal angles $0 \leq \psi \leq \pi$ where ψ is the angle between the wave normal and the ambient magnetic field, assuming that the wave normal lies in the meridional plane defined by the direction of $\mathbf{B}_0$ and the x axis, where the x axis is assumed to be normal to the planar surface of the irregularity.

In analogy with Figure 1, we assume that the refractive index surface applies to region I with density N_1 and that a similar refractive index surface applies in region II where $N = N_2$. In region I we assume that an electromagnetic whistler mode wave (IW) is incident on the boundary between the two media at a small angle with respect to the z axis. Applying Snell's law at the boundary, i.e., $n_z = n_{zi}$, we find the four possible values for n from the intersection of the $n_z = n_{zi}$ line with the refractive index surface. The sketch shows the case for which $\chi > \chi_c$. Comparing Figures 1 and 6 we see that one of the four possible solutions lies on the lower half sheet of the refractive index surface at the point labeled d. This solution represents a wave whose group velocity along $\mathbf{B}_0$ is in the opposite direction from that of the input wave. This "backward" wave has a group velocity vector pointing toward negative x, the opposite direction from the group velocity of the input wave. Assuming

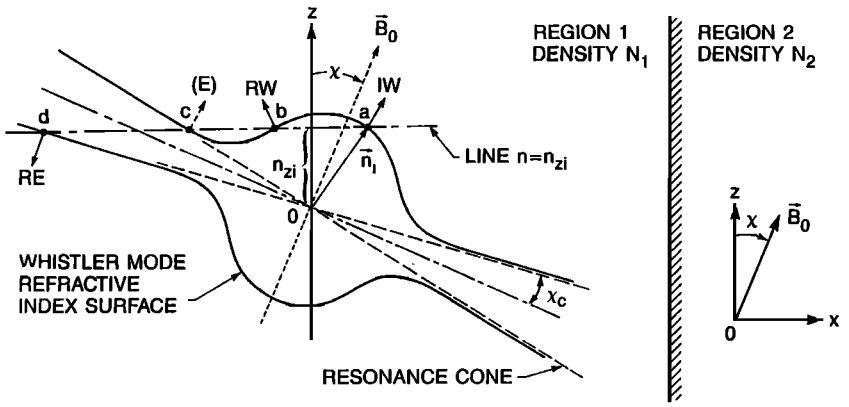

Fig. 6. Schematic representation showing an electromagnetic whistler mode wave scattering from a single sharp boundary surface which is tilted at an angle χ with respect to $\mathbf{B}_0$. Only the case $\chi > \chi_c \equiv \pi/2 - \psi_r$ is shown.

that the density enhancement in medium II is small, the refractive index surface in this medium will resemble Figure 6 very closely and the four solutions for n will be close to those shown in Figure 6. We label these four solutions, a', b', c', and d'. In this case we see that the appropriate solution in medium I consists of a sum of the incident electromagnetic whistler mode wave (a), the reflected (RW) electromagnetic whistler mode wave (b), and the "reflected" lower hybrid wave (d). Within medium II the appropriate solution consists of a sum of the transmitted electromagnetic wave (a') and the "transmitted" lower hybrid wave (c'). Thus in medium II all excited waves propagate along $\mathbf{B}_0$ in the same direction as the incident wave, while in medium I the electromagnetic and lower hybrid waves propagate in the opposite direction along $\mathbf{B}_0$.

In this more general case, we can rewrite the dispersion relationship in each medium in terms of the unknown n_x in the following way:

$$\alpha_4 n_x^4 + \alpha_3 n_x^3 + \alpha_2 n_x^2 + \alpha_1 n_x + \alpha_0 = 0 \tag{16}$$

where

$$\alpha_4 = S\cos^2\chi + P\sin^2\chi$$
$$\alpha_3 = (P-S)n_z \sin 2\chi$$
$$\alpha_2 = (S+P)n_z^2 + \left[S(1+\cos^2\chi) + P\sin^2\chi\right]n_y^2 - RL\cos^2\chi - PS(1+\sin^2\chi)$$
$$\alpha_1 = (n_z \sin 2\chi)\left[(P-S)(n_y^2+n_z^2) + RL - PS\right]$$
$$\alpha_0 = S(n_y^2+n_z^2)(n_y^2+n_z^2\sin^2\chi) + Pn_z^2(n_y^2+n_z^2)\cos^2\chi - PS\left[n_y^2 + n_z^2(1+\cos^2\chi)\right] + PRL - RL(n_y^2+n_z^2\sin^2\chi)$$

and where, by Snell's law $n_z = n_{zi}$ and $n_y = n_{yi}$ with the subscript i referring to the incident wave.

Equation (16) is one form of the Booker quartic relationship [*Budden*, 1985] and each of the four possible solutions determines a normal mode of the system. The polarization ratios of each normal mode have the values

$$\rho_0\rho_y = -iD\left[(P - n_x^2 - n_y^2)\cos\chi + n_x n_z \sin\chi\right] + n_y\left[n^2 n_x - (n_x\sin\chi + n_z\cos\chi)S\sin\chi + (n_z\sin\chi - n_x\cos\chi)P\cos\chi\right] \tag{17a}$$

$$\rho_0\rho_z = n_x n_z(n^2 - S) + iDn_y(n_x\sin\chi + n_z\cos\chi) + \tfrac{1}{2}(\sin 2\chi)\left[RL - SP + (P-S)(n^2 - n_y^2)\right] \tag{17b}$$

$$\rho_0 \equiv (S-n^2)(P\cos^2\chi - n_x^2) + n_y^2(P\cos^2\chi - S) + \left[RL + S(n_y^2 - n^2)\right]\sin^2\chi \tag{17c}$$

where $\rho_y \equiv E_y/E_x$ and $\rho_z \equiv E_z/E_x$.

In the present work we are concerned with wave frequencies which are small compared to the electron gyrofrequency f_{He}, in particular the range $f_{LHR} \lesssim f \leq 30$ kHz. When $f = f_{LHR}$, the resonance cone half angle has the value $\psi_r = 90°$, while for 30-kHz waves with $f_{He} = 880$ kHz, $\psi_r \approx 88°$. Thus the tilt angle need only be a few degrees in order to change the character of the stimulated lower hybrid waves. For small values of χ, the four roots of (16) can be approximated by the relations

$$n_x^{ES} \sim \frac{-\alpha_3 \pm \sqrt{\alpha_3^2 - 4\alpha_4\alpha_2}}{2\alpha_4}$$
$$n_x^{WM} \sim \frac{-\alpha_1 \pm \sqrt{\alpha_1^2 - 4\alpha_2\alpha_0}}{2\alpha_2} \tag{18}$$

One of the characteristics of plane electrostatic waves is that $\mathbf{E}$ is parallel to $\mathbf{k}$. A common definition of a quasi-electrostatic plane wave is one in which $|E_\perp| \ll |E_\parallel|$, where $E_\perp$ is the component of $\mathbf{E}$ perpendicular to $\mathbf{k}$ and $E_\parallel$ is the component parallel to $\mathbf{k}$. From the polarization relations (17) it can be shown that for the parameters of the present study we have $|E_\perp| \ll |E_\parallel|$ whenever $|n_x| \gg |n_z|$. However, when $|n_x| \gg |n_z|$ and $|\chi| \approx \chi_c$, the largest magnitude root of (16) can be approximated by the first two terms of this equation and has the value

$$n_x \cong n_z(S-P)\left(S\cos^2\chi + P\sin^2\chi\right)^{-1}\sin 2\chi \tag{19}$$

Using (19) to find the ratio n_z/n_x to first order in $(\chi - \chi_c)$ we obtain

$$|n_z/n_x| \cong |\chi - \chi_c| \tag{20}$$

where χ is measured in radians.

Let us define the quasi-electrostatic waves of interest in the present work to be those for which $|n_x| \gtrsim 10|n_z|$. In this case from (20) we find

$$|\chi - \chi_c| \lesssim 6° \tag{21}$$

At low altitudes, for frequencies in the range $10 \leq f \leq 30$ kHz, $\chi_c \leq 2^\circ$, and thus the range of tilt angles for which lower hybrid waves can be stimulated is quite small. This fact supports the hypothesis that the lower hybrid waves are stimulated in regions where the plasma density irregularities are closely aligned with the direction of the Earth's magnetic field.

Solutions to the wave equation for the case of tilted irregularities proceed exactly along the lines described above for the case of irregularities which are aligned with $\mathbf{B}_0$. In each slab the solution can be written as in (10), but now the k_x values for the four normal modes are implicitly defined by (16) rather than (10), and the polarization ratios are defined by (17) rather than (14). The scheme of Figure 5*b* still applies and the problem can again be cast into the form $\underline{\mathbf{A}}\,\mathbf{E}_x = \mathbf{C}$, where $\underline{\mathbf{A}}$ is a $4M \times 4M$ matrix with only $32M - 12$ nonzero entries for $M \geq 2$.

3. RESULTS

Below we present the results of the above formulation as applied to a range of magnetospheric conditions.

Magnetic-Field-Aligned Plasma Density Irregularities

Since we will approximate each electron density irregularity by a large number of constant density planar slabs, as illustrated in Figure 5*a*, it is instructive to consider the lower hybrid wave excitation that can occur at a single boundary between two slabs of different density. An example of the results of (13) and (15) for the single boundary case is shown in Figure 7 for the case in which a whistler mode wave of 15-kHz frequency with wave normal in the x-z plane is incident at a polar angle of 10° with respect to the magnetic-field-aligned planar boundary between the two semi-infinite cold magnetoplasmas. Since $\mathbf{B}_0$ is along z, the wave normal angle is also 10°. In the first medium the plasma parameters have the following values:

$$\begin{aligned} f_{0e} &= 2 \text{ MHz} \\ f_{He} &= 880 \text{ kHz} \\ \alpha(\mathrm{H}^+) &= 20\% \\ \alpha(\mathrm{O}^+) &= 80\% \\ f_{LHR} &\approx 9.8 \text{ kHz} \end{aligned} \tag{22}$$

where $\alpha(\mathrm{H}^+)$ is the percentage of hydrogen ions and $\alpha(\mathrm{O}^+)$ is the percentage of the oxygen ions. In the second medium $f_{0e} = 2.05$ MHz, consistent with a 5% plasma density enhancement, while all other parameters are the same as given in (22). These parameters are consistent with conditions that are common near 1000 km altitude within the plasmasphere near $L \sim 3.5$. The top two panels of the figure show, at a fixed moment in time, the spatial variation of the real and imaginary parts of the x component of the electric field of the incident electromagnetic whistler mode wave propagating to the right (dashed curve), the reflected electromagnetic whistler mode wave propagating toward the left (chain-dash curve), the stimulated quasi-electrostatic lower hybrid wave propagating toward the left (dotted curve), and the stimulated quasi-electrostatic lower hybrid wave propagating toward the right (solid curve). The bottom panel shows the cold plasma density enhancement, $\Delta N/N_0$, where N_0 is the cold plasma density in the left-hand medium $x < 0$ and ΔN is the enhancement of density in the right-hand medium

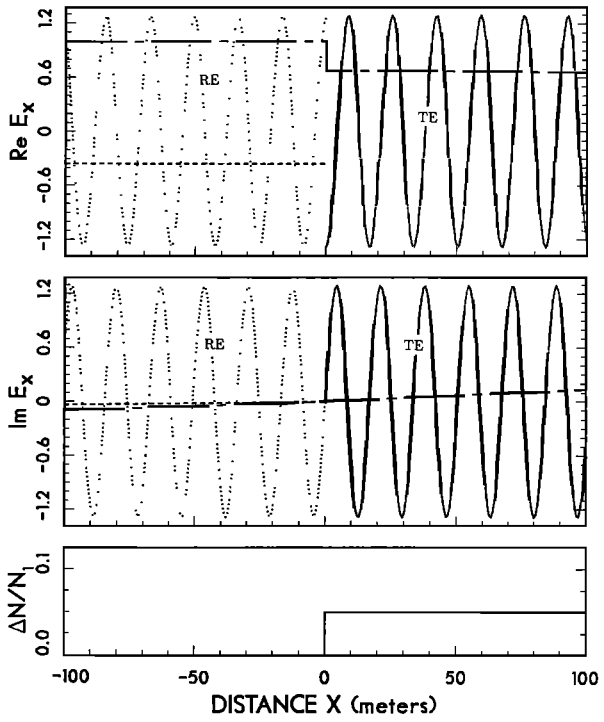

Fig. 7. Simulation result for an incident electromagnetic whistler mode wave scattering from a single sharp boundary. Plasma parameters: electron plasma frequency $f_{0e} = 2$ MHz, electron gyrofrequency $f_{He} = 880$ kHz, density enhancement $\Delta N/N_0 = 5\%$, 80% O^+, 20% H^+, tilt angle $\chi = 0$. Wave parameters: $f = 15$ kHz, $\theta_{INC} = 10^\circ$, $\phi_{INC} = 0$. Bottom panel shows the density enhancement profile $\Delta N(x)/N_0$. Top and middle panels show a snapshot of the real and imaginary parts of the electric field component normal to the boundary surface for each of the four propagating whistler mode waves. Chain-dash (dash) curve: right (left) propagating electromagnetic whistler mode wave. Solid (dotted) curve: right (left) propagating stimulated quasi-electrostatic lower hybrid wave.

$x > 0$. In the top two panels all amplitudes are normalized to the amplitude of the incident electromagnetic whistler mode wave at $x = 0$. The electromagnetic components do not vary significantly where $x \neq 0$ since the horizontal scale is only a fraction of a wavelength for these waves.

It can be seen that the amplitudes of both the right and left propagating lower hybrid waves exceed that of the incident wave even though the density enhancement is only 5%. Furthermore, the wavelength of the stimulated lower hybrid waves is roughly 17 m, much smaller than the ~ 1-km wavelength of the electromagnetic whistler mode waves.

The dependence of the stimulated lower hybrid wave amplitude E_x^{ES} upon the frequency of the incident electromagnetic whistler mode wave is shown in Figures 8*a*, 8*b*, 8*c*, and 8*d* for four values of the density enhancement $\Delta N/N_0 =$ 5%, 10%, 20%, and 100%, and for the incident wave normal angle of 10° with respect to the planar boundary. (Note that evanescent waves were not plotted. For instance, the chain-dash curve in Figure 8*d* shows that the excited waves are evanescent when the incident wave frequency falls below ~ 2.5 kHz or exceeds ~ 16 kHz.) Figure 8*a* pertains to the plasma conditions given in (22), Figure 8*b* pertains to the topside ionosphere near $L \sim 3$, Figure 8*c* pertains to 1400 km altitude in the subauroral region, and Figure 8*d* pertains to altitudes above 3000 km within the inner radiation belt near the equator. Figures 8*b*–8*d* will be discussed in section

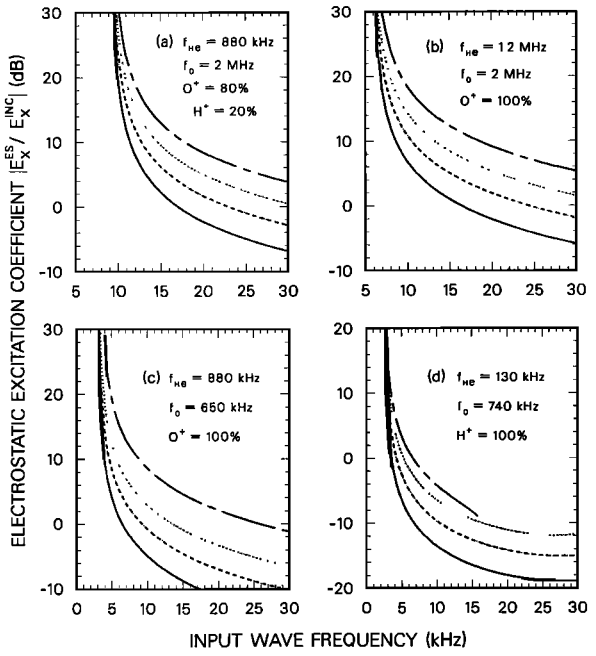

Fig. 8. Normalized amplitude of the lower hybrid wave excited in the region $x > 0$ as a function of input wave frequency under typical plasma conditions (a) at 1400 km altitude within the plasmasphere near $L \sim 3.5$, (b) in the topside ionosphere, (c) in the subauroral region, (d) in the inner radiation belt. Four values of density enhancement are shown in each panel: $\Delta N/N_0$ = 5% (solid curve), 10% (dash curve), 20% (dotted curve), 100% (chain-dash curve).

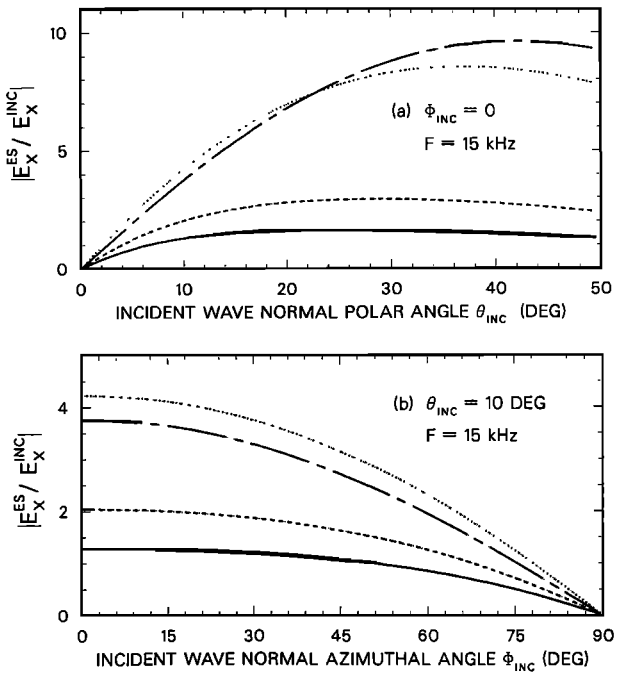

Fig. 9. Normalized amplitude of the lower hybrid wave stimulated in the region $x > 0$ as a function of (a) input wave normal polar angle θ_{INC} with azimuthal angle ϕ_{INC} held fixed at 0, and (b) input wave normal azimuthal angle ϕ_{INC} with θ_{INC} held fixed at 10°. Four values of density enhancement are shown: $\Delta N/N_0$ = 5% (solid), 10% (dash), 50% (dotted), 200% (chain-dash).

4. From Figure 8a it can be seen that E_x^{ES} is comparable to the amplitude of the incident wave for most values shown for the density ratio and incident wave frequency. For the cold plasma model we have chosen, E_x^{ES} increases without bound as $f \rightarrow f_{LHR}$ from above, as suggested in the figure. However the inclusion of thermal effect will modify this result, as will be shown in a later section. For $f < f_{LHR}$, no lower hybrid waves are stimulated since no resonance cone exists in this frequency range for whistler mode waves.

The dependence of E_x^{ES} upon the wave normal angle θ_i of the incident electromagnetic whistler mode wave is shown in Figure 9a for the case $f = 15$ kHz assuming that (22) applies. For a given level of density enhancement, E_x^{ES} reaches a maximum value when θ_i lies in the range $30° \lesssim \theta_i \lesssim 40°$.

Figure 9b shows the case when the wave normal of the incident wave is oriented at an arbitrary angle with respect to the x-z plane. It can be seen that there is little dependence upon ϕ_i for small values of $\Delta N/N_0$.

We have used the boundary conditions of (11) in order to determine E_x^{ES} for given input conditions. Our results show that E_x^{ES} can exceed the amplitude of the input electromagnetic whistler mode wave for a wide range of density enhancement, angle of incidence, and wave frequency. Furthermore, we have assumed a cold magnetoplasma model which has no free energy to contribute toward wave growth. How then can E_x^{ES} exceed the amplitude of the input wave without violating the law of conservation of energy?

To answer this question, we first note that the use of (11) ensures conservation of energy for the waves, since the complex Poynting flux P_x along the x axis is just $P_x = \frac{1}{2}[E_y H_z^* - E_z H_y^*]$ and each of these field quantities is continuous across $x = 0$ according to (11). Thus $P_x|_{x=0-} = P_x|_{x=0+}$ and energy is conserved along the x direction. However, since the stimulated electrostatic lower hybrid waves have very small values of magnetic field, large values of electric field are possible for these waves even though they may carry much less electromagnetic energy than the incident electromagnetic wave.

An equivalent way to view the situation is to note that the energy stored in the **E** and **H** fields of the incident wave is convecting toward the planar boundary at the group velocity V_{Gx}^{IW}. On the other hand, energy in the **E** field of the quasi-electrostatic waves is convected away from the planar boundary with the group velocity V_{Gx}^{ES}. In general, when $f_{LHR} \lesssim f \ll f_{He}$, it is found that $|V_{Gx}^{ES}| \ll |V_{Gx}^{IW}|$. Because V_{Gx}^{IW} is so small, the electric field energy density of the quasi-electrostatic waves must be large in order to transport measurable energy from the boundary. A further discussion of the Poynting flux of the lower hybrid waves can be found in section 5. Numerical values are given in Figure 22.

Figure 10 shows a plot of the group velocity of the stimulated waves along both the x and z ($\mathbf{B}_0$) directions as a function of frequency, normalized to the value of the group velocity of the incident wave in the same direction. The plasma parameters are as given in (22). Two values of wave normal angle θ_i are considered. The relative group velocity of the quasi-lower hybrid waves in the x direction is always less than 5×10^{-2} for $f < 15$ kHz. The relative group velocity in the direction of $\mathbf{B}_0$ is always less than 0.2 for $f_{LHR} \lesssim f < 12$ kHz. However for higher frequencies, the relative group velocity in the direction of $\mathbf{B}_0$ approaches 0.5.

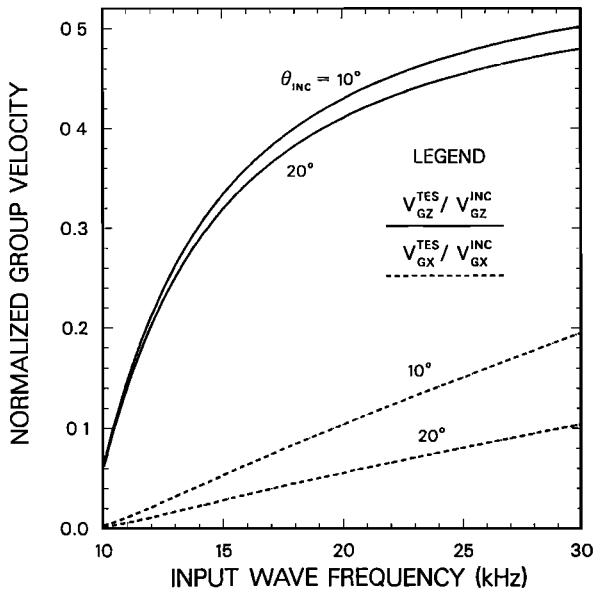

Fig. 10. Normalized group velocity of the lower hybrid wave excited in region the $x > 0$ as a function of input wave frequency. Components parallel and normal to the field-aligned irregularity boundary are shown separately.

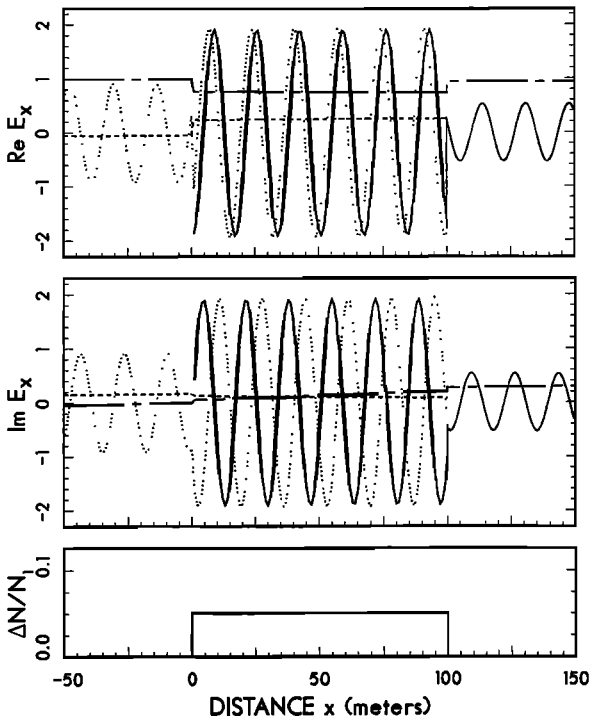

Fig. 11. Simulation result showing a snapshot of the normalized electric field for the case of a 15-kHz electromagnetic whistler mode wave scattering from a constant density enhancement slab of 100 m thickness. Curve format and other plasma and wave parameters are the same as in Figure 7.

The foregoing results apply to the case of a single planar boundary. In the more general case where the density irregularity is distributed over a length W, we can approximate the actual distribution by a series of constant density slabs as shown in Figure 5. If the number of slabs is sufficiently large, the approximate solution approaches the exact solution.

Distributed Irregularity

As the simplest example of a planar irregularity with density distributed over a length W, we consider the case in which the planar irregularity consists of a slab of constant plasma density N_2 which occupies the region $0 \leq x \leq W$. In the remaining space ($x < 0$ and $x > W$) the plasma density has the constant background value of N_0. It is assumed that the ambient magnetic field and ionic composition are constant for all x.

With this configuration of just two planar surfaces of discontinuity, application of the boundary conditions (11) at each boundary leads to a system of 8 equations in 8 unknowns. Figure 11 shows the results of the solution of the 8×8 matrix equation for the case of a 5% density enhancement density within the slab and with the other plasma parameters identical to those listed in (22).

The two upper panels of Figure 11 show the real and imaginary parts of the x-directed electric fields of the incident electromagnetic whistler mode wave (chain-dash curve in the region $x \leq 0$), the reflected electromagnetic whistler mode wave (dashed curve), the "reflected" lower hybrid wave (dotted curve), the transmitted electromagnetic whistler mode wave (chain-dash curve in the region $x \geq 0$), and the "transmitted" lower hybrid wave (solid curve). The bottom panel shows a plot of the density enhancement of the slab along the x axis.

There are some features of Figure 11 which arise because of the presence of the second boundary at $x = 100$ m. First of all, the amplitudes of the "reflected" and "transmitted" lower hybrid waves are not roughly equal as they are in Figure 7. Second, the amplitude of the lower hybrid waves is significantly larger within the planar irregularity than without. These differences arise because of multiple reflections of waves within the irregularity which lead to constructive and destructive interference effects at the boundaries.

Comparing Figures 11 and 7 it is found that the amplitude of the reflected electromagnetic whistler mode wave is much smaller for the two-boundary finite-width irregularity than for the single boundary case. This difference arises because of destructive interference between the electromagnetic waves reflected from the two boundaries in Figure 11. Since the spacing between the two boundaries is much smaller than the wavelength of the electromagnetic whistler mode wave, the electromagnetic wave experiences a scattering that is analogous to that of an electromagnetic wave in an isotropic dielectric medium which encounters an optically thin dielectric slab [*Born and Wolf*, 1970]. In essence a reflected electromagnetic wave is excited at each of the two boundaries of the slab. These two waves are of similar magnitude but are 180° out of phase. As a result of this difference the sum of the two reflected waves at $x = 0$ is greatly reduced. Thus it can be seen that irregularities whose scale is much less than that of the wavelength of the electromagnetic whistler mode wave will reflect very little electromagnetic whistler mode wave energy even though significant excitation of lower hybrid waves takes place.

Thus far we have considered the stimulation of lower hybrid waves by irregularities whose boundaries are assumed to be very sharp. This assumption is questionable when considering scales of the order of meters since the thermal H^+ and O^+ gyroradii are generally of this same order. Thus we

need to consider the lower hybrid wave stimulation mechanism when the boundary of the irregularity is smoothly varying. In order to address this question in as simple a manner as possible, we reconsider the case in which we have only a single boundary between two regions of cold plasma density $N_1 \equiv N_0$ and N_2, and we join the two levels smoothly in a boundary layer of width l which begins at $x = 0$. The varying density $N(x)$ in the boundary layer is assumed to have one of the following forms:

Linear model:

$$N_a(x) = N_0 + (x/l)\Delta N \tag{23a}$$

Sinusoidal model:

$$N_b(x) = \tfrac{1}{2}\left[N_0 + N_2 - \Delta N \cos(\pi x/l)\right] \tag{23b}$$

Quartic model:

$$N_c(x) = N_0 + \left[4(x/l)^3 - 3(x/l)^4\right]\Delta N \tag{23c}$$

Gaussian model:

$$N_d(x) = N_0 + \Delta N\left[\frac{e^{-\alpha(x/l-1)^2} - e^{-\alpha}}{1 - e^{-\alpha}}\right] \tag{23d}$$

where $\Delta N \equiv N_2 - N_0$.

All the above models are continuous in $N(x)$ over the entire x axis, however they differ in smoothness at the two edges of the boundary layer, $x = 0$ and $x = l$. Model a has a discontinuous first derivative $(dN(x)/dx)$ at the edge points. Model b has continuous first derivative at the edge points but discontinuous second derivative there. Model c has continuous first and second derivatives at $x = 0$ and continuous first derivative at $x = l$. Model d, in principle, has discontinuous first and higher order derivatives at $x = 0$, but these discontinuities can be made arbitrarily small by increasing the parameter α. The values of $N(x)$ associated with each model are plotted in Figure 12. It can be seen that the smoothness of increase of $N(x)$ at $x = 0$ corresponds to the ranking of (23).

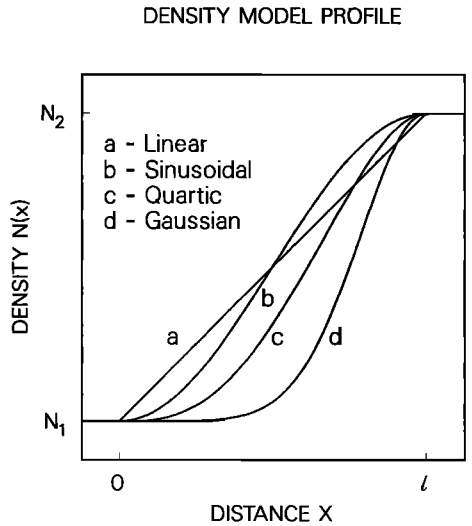

Fig. 12. Refinement of the single sharp boundary model. The density varies continuously from the background value N_0 at $x = 0$ to $N_2 = N_0 + \Delta N$ over a distance l, the boundary layer width. Four density profiles are shown.

In performing calculations using the above models, the region $0 \leq x \leq l$ was divided into 1000 slabs of constant density as indicated in figure 5. For model d it was assumed that the density enhancement $\Delta N(x) = N(x) - N_0$ reaches one half its maximum value at $x = 3l/4$. Thus for this case $\alpha = 11.1$. In all cases it was assumed that (22) holds.

Figures 13a and 13b show the results of calculations involving the above four models for the boundary layer where the total density change across the layer is 5%. The amplitude of the electric field of the lower hybrid waves "reflected" from the boundary layer is shown as a function of the normalized width l/λ_{ES} of the boundary layer. The field amplitude is shown for two frequencies, $f = 10$, and 15 kHz, for which the wavelengths of the lower hybrid waves are roughly 6 m and 17 m, respectively. In each figure it can be seen that each boundary layer model yields the same values for E_x^{ES} when $l \to 0$, i.e., as the width of the boundary layer approaches zero. Furthermore, these values for E_x^{ES} are identical to those calculated for the case of a single sharp boundary, as shown in figure 7. It can be seen that the amplitude of the stimulated lower hybrid wave for each model is approximately equal to its value for the sharp boundary case $(l \to 0)$ as long as l is less than one half wavelength of the lower hybrid wave. This condition was found to be true for all frequencies in the range $f_{LHR} \lesssim f \leq 30$ kHz.

It is interesting to note that models a, b, and c show amplitude variations that have a scale in l of one lower hybrid wavelength. Presumably, this is due to constructive and destructive interference of stimulated lower hybrid modes at the edges of the boundary layer. The amplitude variations are smaller for the models which have a smoother increase in $N(x)$ at $x = 0$. Model d, the Gaussian model, produces no discernable amplitude variation with a wavelength scale.

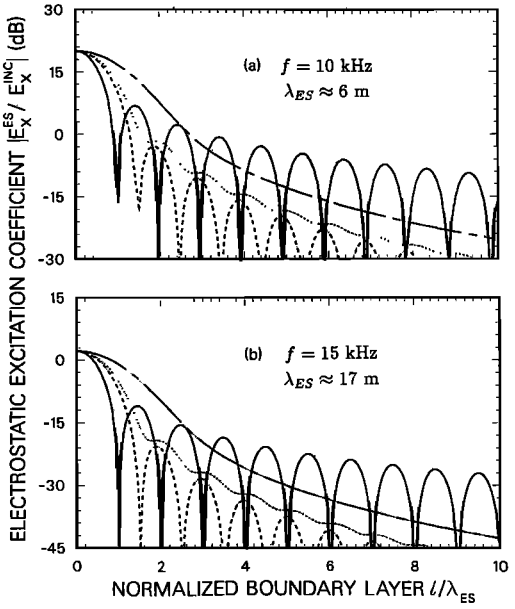

Fig. 13. Normalized amplitude of the lower hybrid wave excited in the region $x < 0$ as a function of the normalized boundary layer width l/λ_{ES} for the four density models depicted in Figure 12. The input wave frequency f =(a)10 kHz and (b) 15 kHz. Solid curve: linear model. Dash curve: sinusoidal model. Dotted curve: quartic model. Chain-dash curve: Gaussian model. Plasma and other wave parameters are the same as in Figure 7.

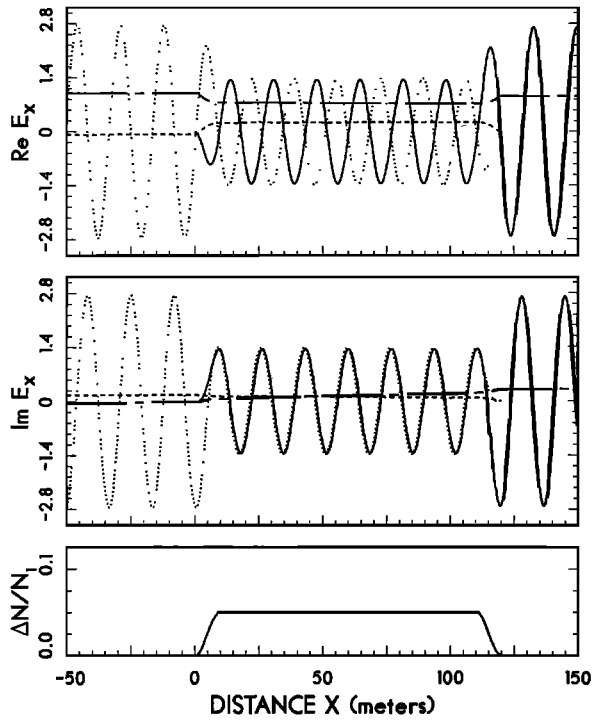

Fig. 14. Simulation result for a snapshot of the normalized electric field for the case of an incident electromagnetic whistler mode wave scattering from an irregularity slab with two sinusoidally varying boundary layers of 10 m width. Curve format and plasma and wave parameters are identical to those in Figure 7.

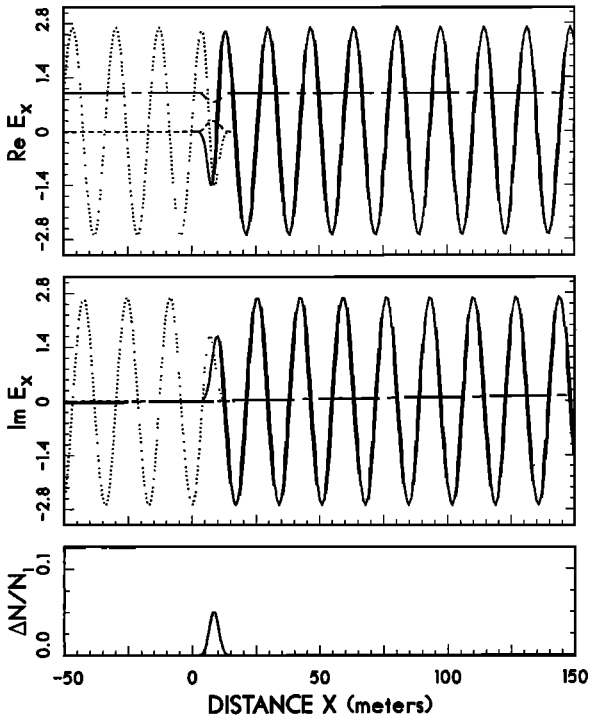

Fig. 15. A snapshot of the normalized electric field for the case of an incident electromagnetic whistler mode wave scattering from a single Gaussian density enhancement of FWHM $= \lambda_{ES}/4 \approx 4.25$ m and peaking at $x \approx 8.5$ m. Curve format and other plasma and wave parameters are identical to those in Figure 7.

Figure 14 shows an example of a case of an irregularity with two smoothly varying boundaries. The irregularity is comprised of a constant density core of 100 m width joined to the ambient plasma density with sinusoidally varying boundary layers of 10 m width identical in form to that plotted in curve *b* of Figure 12 and (23). The plasma parameters and angle of incidence are identical to those of Figure 11. Comparing the two figures it can be seen that the stimulated wave amplitude outside the irregularity is larger for the irregularity with smoothly varying boundaries. This feature results from constructive interference of the stimulated waves.

In order to stimulate lower hybrid waves of significant amplitude, the irregularity must have a minimum width W which is comparable to the wavelength, λ_{ES}, of the stimulated waves. If $W \ll \lambda_{ES}$, the irregularity will be optically thin to the lower hybrid waves and their amplitude will be proportional to the ratio W/λ_{ES}, as discussed in connection with the electromagnetic case above. This feature is illustrated in Figures 15 and 16. Figure 15 shows the amplitude of the lower hybrid waves stimulated as the incident electromagnetic whistler mode wave encounters an irregularity with a Gaussian shape whose full width at half maximum, d, has the value $\lambda_{ES}/4$, where in this instance $\lambda_{ES} = 17$ m.

Figure 16 shows the amplitude of the lower hybrid waves stimulated as the incident electromagnetic whistler mode wave encounters a Gaussian shaped density irregularity of arbitrary d, for the range $0 \leq d \leq 16$ m. The plasma parameters are the same as given in (22). The amplitude of the stimulated waves reaches a maximum at $d \approx 6$ m. The amplitude of the stimulated waves is decreased significantly when $d < \lambda_{ES}/8$, where in this case $\lambda_{ES} \approx 17$ m. Results at other frequencies are similar, leading to the conclusion

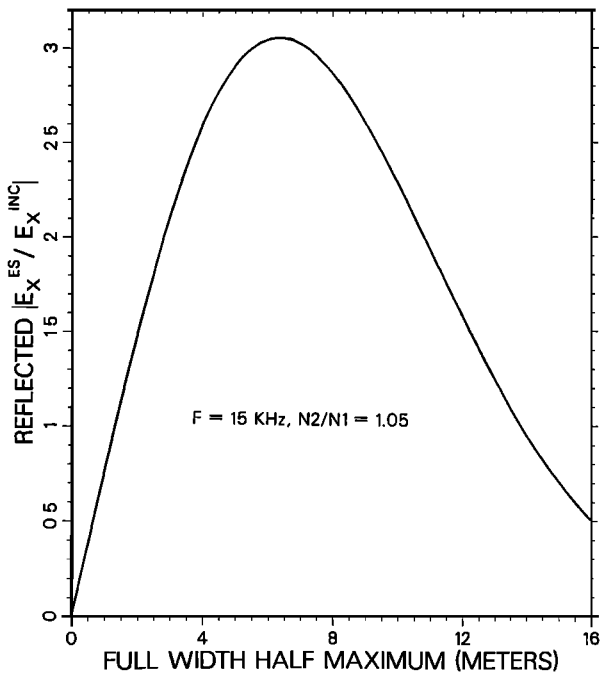

Fig. 16. Normalized amplitude of the lower hybrid wave stimulated in the region $x < 0$ as a function of the full width at half maximum of the Gaussian density enhancement. Other wave and plasma parameters are identical to those in Figure 15.

that a necessary condition for the excitation of lower hybrid waves is that the full width of the irregularity be no smaller than roughly one eighth wavelength. It can be seen that the stimulated wave amplitude is a linear function of d for $d < \lambda_{ES}/4$.

Multiple Irregularities With Periodic Spacing

The results of Figures 15 and 16 demonstrate that lower hybrid waves of significant amplitude can be produced in the presence of irregularities with small density enhancement and width. It is of interest to determine whether these same amplitude levels can be achieved by a spatially distributed array of irregularities of much smaller enhancement but similar width. Figure 17 shows such a case in which irregularities with Gaussian density distribution are distributed along the x axis with a spacing equal to the lower hybrid wavelength of $\sim$ 17 m. Each Gaussian density enhancement is identical to that shown in Figure 15, except that the peak density of each Gaussian in Figure 17 is one tenth the peak density of the Gaussian shown in Figure 15. As a result of the smaller enhancement value, the amplitude of the lower hybrid waves excited at each density perturbation is roughly one-tenth of the value shown in Figure 15. However, since the spacing between the Gaussians is equal to one lower hybrid wavelength, the stimulated waves from each perturbation add in phase and the final stimulated wave amplitude is the sum of the individual amplitudes. Thus the final stimulated wave amplitude in Figure 17 is the same as that in Figure 15.

This behavior suggests that the stimulated lower hybrid waves can be used as a diagnostic tool to determine the properties of the irregularities within which they are excited. This idea is discussed further in section 4.

Effects of Tilt Angle

In order to show the effects of the tilt angle χ upon the excitation coefficient of the lower hybrid waves we consider the single boundary case in which the density enhancement in medium II is 5% and all other parameters are as given in (22). The normalized amplitude of the lower hybrid wave excited in medium I is shown in Figure 18 for three frequencies, 10, 15, and 30 kHz. Figure 18(a) shows the normalized amplitude of the excited lower hybrid wave, while Figure 18(b) shows the group velocity of the excited lower hybrid wave along $\mathbf{B}_0$. In medium I, $E_x^{ES} \rightarrow \infty$ as $\chi \rightarrow \chi_c$ and $n_x^{ES} \rightarrow \infty$ (Similarly in medium II, $E_x^{ES} \rightarrow \infty$ as $\chi \rightarrow -\chi_c$ and $n_x^{ES} \rightarrow \infty$.). As discussed in connection with Figure 6, the group velocity of the lower hybrid and input electromagnetic wave in medium I along $\mathbf{B}_0$ have the same direction for $\chi < \chi_c$ but the opposite direction for $\chi > \chi_c$.

The figure demonstrates that, at all frequencies shown, the existence of a small tilt angle can dramatically increase the amplitude of one branch of the stimulated lower hybrid waves. Although the figure shows essentially unbounded values of $|E_x^{ES}|$ near the critical tilt angle, this result applies only to the case of a cold plasma. In section 5 we discuss how thermal effects will modify this behavior. Although Figure 18 is plotted for the case $k_y = 0$, the results are insensitive to finite values of k_{yi} as long as $k_{yi}^2 \leq k_{xi}^2$. This behavior is similar to that shown in Figure 9b.

The group velocity of the stimulated lower hybrid waves along $\mathbf{B}_0$ is also a rapidly varying function of the tilt angle for $10 \leq f \leq 30$ kHz. This behavior is illustrated in Figure 18b for the lower hybrid wave in medium I for the single boundary case. Similar behavior is found for medium II. The lower hybrid waves excited when $|\chi| \approx \chi_c$ propagate much more slowly along $\mathbf{B}_0$ than those excited when $\chi \approx 0$. Thus the excited waves of highest amplitude will exhibit the largest relative time delay at the observation point.

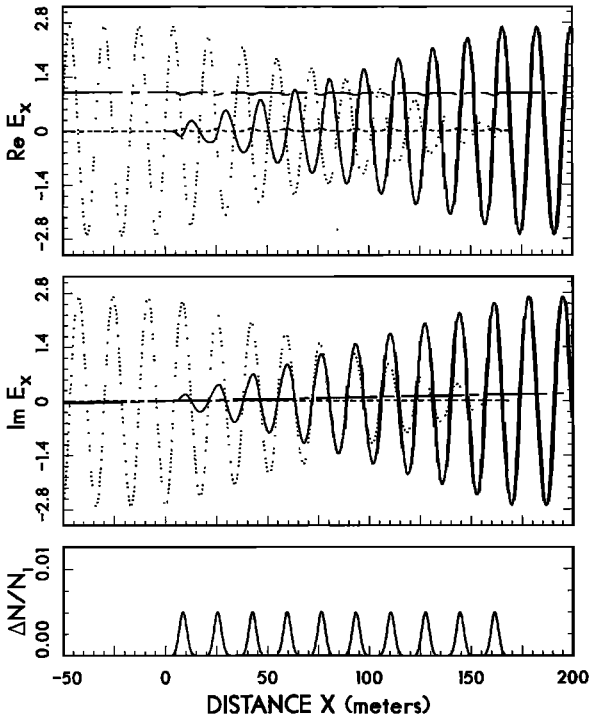

Fig. 17. A snapshot of the normalized electric field for the case of an incident electromagnetic whistler mode wave scattering from 10 Gaussian density enhancements, each identical in width to that shown in Figure 15 but with only 1/10 of the amplitude. The enhancements are equally spaced at a distance $\lambda_{ES} \approx 17$ m. Curve format and other plasma and wave parameters are identical to those in Figure 15.

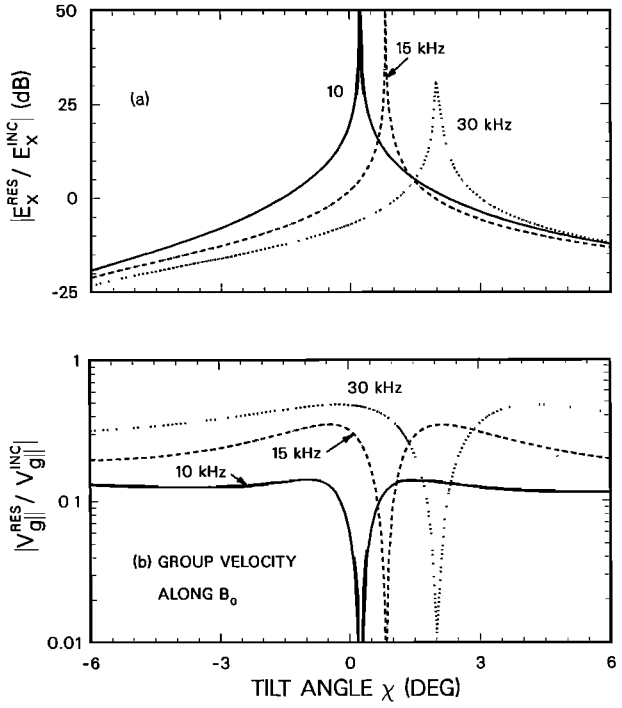

Fig. 18. Effect of boundary tilt upon stimulated lower hybrid waves as a function of tilt angle χ. (a) Normalized amplitude of lower hybrid wave stimulated in region $x < 0$. (b) Normalized group velocity component along $\mathbf{B}_0$ of lower hybrid wave stimulated in region $x < 0$.

4. APPLICATIONS

4.1. *Satellite Data*

In a recent paper [*Bell and Ngo*, 1988] it was shown how the Doppler shift of stimulated lower hybrid waves observed on the ISEE 1 satellite in the inner radiation belt could be explained using the proposed stimulation mechanism outlined above. Furthermore, both the Doppler shift and time delay of stimulated lower hybrid waves observed on the ISIS spacecraft at mid-latitude were also shown to be consistent with the proposed stimulation mechanism [*Bell et al.*, 1983; *James and Bell*, 1987].

If the physical characteristics of existing plasma density irregularities had been measured during these satellite observations, one could use the results of section 3 to calculate the predicted amplitude of the stimulated lower hybrid waves and a direct comparison could be made between theory and observation. Unfortunately, the irregularity structure was not measured on either the ISEE 1 or ISIS satellites during the times that stimulated lower hybrid waves were observed. Thus no definitive test of our theory can be made here. However, it is possible to show at least that the predictions of our theory are consistent with the data.

Strictly speaking, our one-dimensional theory applies only to cases in which lower hybrid waves are excited at planar irregularities. A distinguishing feature of this type of excitation is the fact that the electric vectors of the lower hybrid waves will be oriented roughly perpendicular to the plane of the irregularities. Data suggesting a preferred azimuthal orientation of the lower hybrid wave electric vector about $\mathbf{B}_0$ has been reported by *Bell et al.* [1983] and *James and Bell* [1987]. Plasma parameters during these observations ranged between those shown in Figure 8*b* and 8*c*, and the measured ratio of power in the electric field of the lower hybrid waves to the power in the electric field of the input whistler mode wave generally ranged between 0 and 20 dB.

In theory the total lower hybrid field at a point x produced by weak scattering at M separate planar irregularities (boundaries) can be approximated by the expression

$$E_{xT}^{ES} = \sum_{m=1}^{\ell} E_{xm}^{ES} e^{-ik'(x-x_m)} + \sum_{m=\ell+1}^{M} E_{xm}^{ES} e^{ik'(x-x_m)} \quad (24)$$

where E_{xm}^{ES} is the field excited at the planar boundary located at x_m along the x axis, $k' \equiv k_x^{ES}$, where $x_m > x$ for $1 \le m \le \ell$, and $x_m < x$ for $\ell + 1 \le m \le M$, and where it is assumed that $\chi = 0$.

In (24) it is assumed that the density change at each irregularity is small and that multiple reflections of lower hybrid waves are not important. Because the wave normals of the two sets of waves in (24) have opposite directions, a satellite wave receiver will observe the sets at the apparent frequency, $\omega' = \omega \pm k' v_x$, where v_x is the satellite velocity normal to the irregularities. If the values of x_m are randomly distributed along the x axis, if M is large, if $k'|x_m - x| \gg 1$, and if the ensemble average $< \Delta N > \sim 0$, the time average of the peak electric field intensity observed on a satellite has the approximate value

$$\left|E_{xT}^{ES}\right|^2 \sim \sum_{m=1}^{\ell} \left|E_{xm}^{ES}\right|^2 \delta(\omega' - \omega + k' v_x) + \sum_{m=\ell+1}^{M} \left|E_{xm}^{ES}\right|^2 \delta(\omega' - \omega - k' v_x) \quad (25)$$

where $\delta(\cdot)$ is the Kronecker delta function.

In order to apply (25) to specific examples, we consider ISIS 2 data from August 14, 1979, as discussed in *Bell et al.* [1983]. On this particular day the maximum values of E^{ES}/E^{INC} in the frequency range 10 to 14 kHz were of the order of 20 dB, and the values of the plasma parameters near the scattering region were close to those shown in Figure 8*b*. According to Figure 8*b*, in the 10–14 kHz frequency range, average values of $|E_x^{ES}/E_x^{INC}|$ are roughly 7 dB at $\Delta N/N_0 \sim 10\%$. Thus roughly 40 independent irregularities with $\Delta N/N_0 \sim 10\%$ would be required to reproduce the observations. In this same data set the observed Doppler shifts of the major portion of the lower hybrid waves lay in the range $50 \le f_D \le 300$ Hz, implying wavelengths of roughly $20 \le \lambda_{ES} \le 140$ m.

At the points of observation, the propagation cone half angle had the value $\delta \sim 10^{-2}$ (see Figure 3). If we assume that scattering takes place over a range $\Delta\ell \sim 100$ km, then only irregularities located within the region $\Delta x \sim 1$ km can contribute to the observed lower hybrid field at the spacecraft. In this case the average spacing between irregularities would be 50 m if $\Delta N/N_0 \sim 10\%$. The reasonableness of these numbers is difficult to establish since very little data presently exists concerning the properties of magnetic-field-aligned irregularities of scale less than 100 m at altitudes above the topside ionosphere. However, at lower altitudes, irregularities with scales < 100 m are commonly detected at almost all latitudes [*Fejer and Kelley*, 1980].

If a number of the irregularities in (24) were not spaced randomly along the x axis, but instead were spaced at some integer multiple of the local lower hybrid wavelength, a partially coherent output could be obtained and the number of irregularities necessary to reproduce the observations would be greatly reduced. This question is explored further in section 4.2 below.

As discussed in section 3 above, if an irregularity on which the lower hybrid waves are excited is tilted slightly with respect to $\mathbf{B}_0$, then the lower hybrid waves propagating toward $x > x_m$ will possess a different wavelength and amplitude from that of the lower hybrid waves propagating toward $x < x_m$, where x_m is the location of the irregularity. In general, the stimulated lower hybrid wave of largest amplitude will possess the shortest wavelength, and, hence, the largest Doppler shift. Thus if a set of irregularities all possess the same small tilt, lower hybrid waves excited on these irregularities will display a characteristic signature in which components shifted in frequency in the same direction will possess larger amplitudes and larger Doppler shifts than the components shifted in the opposite direction, resulting in an asymmetric distribution of lower hybrid waves about the input wave frequency. Examples of this type of signature can be found in the August 14 data, e.g., Figure 11*c* of *Bell et al.* [1983], suggesting that tilts may sometimes be an important factor in the stimulation of lower hybrid waves.

To continue our comparison with data, we plot in Figure 19 the total amplitude of stimulated lower hybrid waves to the amplitude of the input electromagnetic wave as a function of time and position along a trajectory of the ISEE 1 satellite through the inner radiation belt (see Figure 10 of *Bell and Ngo* [1988]). During this period the time delay between the arrival of the electromagnetic input wave and the stimulated lower hybrid waves ranged predominantly from 50 to 100 ms, suggesting that the region of stimulation was within a few hundred kilometers of the satellite location. Since the scale for significant change of the plasma frequency

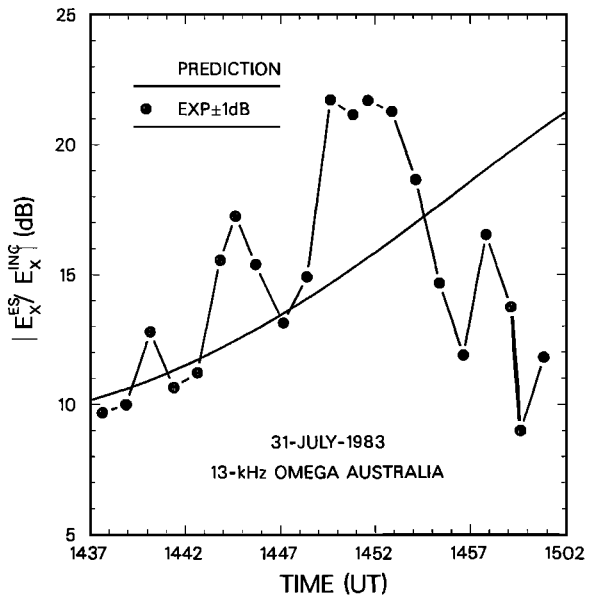

Fig. 19. Comparison of theoretical prediction and experimental measurement of lower hybrid wave amplitude.

and electron gyrofrequency is roughly 1000 km along most of the satellite path, we can expect that the values of these parameters in the stimulation region would be close to those obtaining at the satellite location at any given time. For example, Figure 8*d* gives the calculated excitation coefficient of lower hybrid waves at a particular point along the ISEE 1 satellite path on July 31, 1983 ($L = 2.0$, $\lambda_m = 10^\circ$ N), and we can expect that the excitation coefficient would be close to the values shown for all points within a few hundred kilometers of the spacecraft.

Although we do not know the density enhancements or spatial distribution of the irregularities which produce the observed lower hybrid waves of Figure 19, there is some reason to believe that the observed field will be roughly a constant multiple of the single boundary surface scattering results such as that of Figure 8*d*.

Consider the following argument. If $\Delta N/N_0 \ll 1$, then to first order we can write $E_x^{ES} \approx E_{x0}^{ES} \Delta N/N_0$, where E_{x0}^{ES} is independent of ΔN. At any point along the spacecraft trajectory the observed lower hybrid wave field given in (24) can then be written

$$E_{xT}^{ES} = E_{x0}^{ES} \left\{ \sum_{m=1}^{\ell} \left(\frac{\Delta N_m}{N_0} \right) e^{ik_x^{ES}(x_m - x)} + \sum_{m=\ell+1}^{M} \left(\frac{\Delta N_m}{N_0} \right) e^{-ik_x^{ES}(x_m - x)} \right\} \quad (26)$$

where ΔN_m is the maximum density change associated with the mth irregularity, and x_m is the position of the mth irregularity along the x axis. If we now assume that the irregularities extend significant distances along $\mathbf{B}_0$, some interesting properties of (26) emerge. First of all, we note that the ratios $\Delta N_m/N_0$ remain constant along $\mathbf{B}_0$. Second, since the area of a unit flux tube varies inversely as the magnitude of $\mathbf{B}_0$, the x coordinate of the one dimensional planar irregularities (x_m) will vary roughly as $B_0^{-1/2}$. In this case, from (3) it can be shown that

$$k_x^{ES} |x_m - x_{m-1}| \cong A_m N_0^{1/2} \quad (27)$$

where A_m is a constant along $\mathbf{B}_0$.

In general, at high altitude the background electron density N_0 is a slowly varying function of position along $\mathbf{B}_0$, and the right hand side of (26) will also vary slowly along $\mathbf{B}_0$. Since the same arguments can be applied to the second summation in (24), this result suggests that over a significant distance the observed electrostatic wave field may be a constant multiple of the individual wave field produced at a single irregularity.

In order to test this idea, values of E_x^{ES} were calculated at a number of points along the spacecraft orbit for wave frequency $f = 13$ kHz, assuming $\chi = 0$. Figure 8*d* shows an example of these calculations at the orbital point $L = 2.0$ and $\lambda_m = 10^\circ$ N. At each point the value of the parameter E_{x0}^{ES} was also calculated. The absolute value of each summation in (26) was then chosen to be such that the electric field power given by (26) was equal to the experimental value at this orbital point. The actual value chosen for each summation was $|\sum| = 0.8$, but this is not critical since we are interested mainly in how (26) varies along the orbit. A plot of observed values of $|E_x^{ES}/E_x^{INC}|$ is shown in Figure 19, along with the theoretical values based on (26) .

It can be seen that there is a reasonable agreement between theory and observation until roughly 1455 UT, when the observed values drop significantly below the predicted values. This decrease is believed to be due to the decreased response of the 215-m tip-to-tip electric dipole antenna to the shorter wavelength lower hybrid waves which were excited at the lower altitudes at the end of the satellite pass. On the basis of the Doppler shift of the lower hybrid waves, it can be shown that their wavelength dropped below 100 m after 1455 UT. According to one recent model of the ISEE 1 long electric antenna [*Gallagher*, 1985], the antenna response would be reduced at least 10 dB to waves with $\lambda < 100$ m.

Other differences between the theory and data could result from the fact that the spacecraft trajectory had a significant component across $\mathbf{B}_0$ after 1455 UT. Thus if the irregularity characteristics varied significantly perpendicular to $\mathbf{B}_0$, we would not expect the summation on the right hand side of (24) to remain roughly constant.

In using the results of Figure 8*d* to apply to the ISEE 1 data we have tacitly assumed that the density change at the planar boundary of each irregularity occurs over a distance which is small compared to the lower hybrid wavelength λ_{ES}. This assumption may be reasonable, since in the ISEE 1 data λ_{ES} is relatively large ($\lambda_{ES} > 50$ m). However, if this is not the case and the density change occurs over a distance comparable to, or larger than, λ_{ES}, the excitation coefficient will be smaller, as indicated in Figure 13. In this case the absolute magnitude of the summation in (26) would need to be larger in order to match the observations of Figure 19.

4.2. *VLF "Radar" and Plasma Diagnostics*

In the event that the distribution of the planar irregularities is not entirely random, but instead contains some periodic structures whose spatial wavelength is comparable to the lower hybrid wavelength, we can expect a partially coherent output from the irregularities. This fact is demonstrated in Figure 17. Because of this response, it appears possible to use the lower hybrid wave stimulation effect as a type of "VLF radar" to probe the structure of the irregularities which cause their stimulation.

It is well known from HF incoherent scatter radar studies that HF waves with wavelength in the range 5 to 100 m can

be used to determine the characteristics of plasma density irregularities with roughly the same scale (see, for example, *Brekke* [1977]). For any given component of the irregularity density distribution $N_k e^{-i\mathbf{k}\cdot\mathbf{r}}$, the scattered signal intensity will maximize when the matching condition holds

$$\mathbf{k}_i + \mathbf{k} = \mathbf{k}_s \tag{28}$$

where $\mathbf{k}_i$ and $\mathbf{k}_s$ are the wave vectors of the input and scattered waves, respectively.

The matching condition given in (28) is common to a large class of linear scattering problems including HF incoherent scatter in the ionosphere [*Brekke*, 1977], HF scatter from ocean waves, Bragg scatter of X rays [*Semat*, 1946], and light scattering from atmospheric density variations. It is also applicable to a large class of nonlinear scattering problems, such as parametric three wave interactions, in which the density perturbation is produced by the propagating waves and the frequencies of the three waves are linked by an additional matching condition $\omega_i + \omega = \omega_s$ (see, for example, *Berger and Perkins* [1976]).

In the case of HF incoherent scatter radar studies in which the backscattered signal is observed at the radar site, $\mathbf{k}_s = -\mathbf{k}_i$ and

$$k = 2k_i \tag{29}$$

Thus the maximum backscattered signal will be obtained when the wavelength of the input radar signal is twice the wavelength of the density fluctuation.

Equation (28) can also be applied to the case in which the input signal is an electromagnetic whistler mode wave and the scattered wave is a short wavelength quasi-electrostatic lower hybrid wave excited through mode coupling. If we assume that the Earth's magnetic field $\mathbf{B}_0$ is aligned with the z axis and that the plasma density of the irregularities varies only in the x direction, then (28) becomes

$$k_{iz} = k_{sz} \tag{30a}$$

$$k_{iy} = k_{sy} \tag{30b}$$

$$k_{ix} + k_x = k_{sx} \tag{30c}$$

where k_{iz} is the component of $\mathbf{k}_i$ along the z axis, etc. Equations (30a) and (30b) are just Snell's law applied along the y and z axes. Equation (30c) is the matching condition which produces the maximum amplitude for the scattered lower hybrid wave. Since the wavelength of the input electromagnetic whistler mode wave is much larger than that of the excited lower hybrid wave, $k_{ix} \ll k_{sx}$, and equation (30c) can be expressed to a good approximation:

$$k_x \cong k_{sx} \tag{31}$$

Thus in the case of the excited lower hybrid waves, the maximum amplitude will be achieved when the wavelength of the lower hybrid wave is closely equal to the wavelength of the sinusoidal density fluctuation.

The general relationship between the amplitude of the excited lower hybrid waves and the plasma density profile has been explored in section 3. In general, for large plasma density gradients this relationship is complicated due to strong mode coupling between the two possible electromagnetic modes and the two possible lower hybrid modes and few simplifications seem possible. However, as the input wave frequency approaches the lower hybrid resonance frequency from above, the refractive index of the lower hybrid waves becomes arbitrarily large (in the cold plasma approximation) and the electromagnetic and electrostatic modes partially decouple. In this case as shown in the appendix, in the limit of weak scattering the value of E_x^{ES} is related to the irregularity spectrum $\Delta N(k_x)$ through the relation

$$E_x^{ES}(x)/E_x^{INC} = \rho_y D S^{-1} N_0^{-1} \times \sum_{m=-\infty}^{\infty} \Delta N_m k_m G(k_x^{ES}, k_m, x) \tag{32}$$

where $k_m \equiv 2\pi m/W$, the function G is defined in the appendix, and where we have assumed that the electron density $N(x)$ can be expressed as a Fourier series

$$N(x) = N_0 + \sum_{m=-\infty}^{\infty} \Delta N_m e^{-ik_m x}$$

over the irregularity region of width W.

In principle, if E_x^{ES} can be measured sufficiently accurately, (32) can be solved to find $\Delta N(x)$ by making use of the Fourier inversion relation

$$\delta_{m,n} = W^{-1} \int_0^W e^{ix(k_m - k_n)} dx = \begin{cases} 0 & m \neq n \\ 1 & m = n \end{cases} \tag{33}$$

However, in practice the finite S/N ratio of the lower hybrid waves limits the usefulness of this technique. An alternate method to determine $\Delta N(x)$ involves the measurement of E_x^{ES} over a significant range of values of k_{ES}. This method is based on the fact that, as shown in the appendix, the electric field of the lower hybrid waves will peak when the wave number of the lower hybrid wave is equal to the wave number of one of the spatial Fourier components of the irregularity density distribution $\Delta N(x)$.

Up to the present time, the only controlled experiments involving the excitation of lower hybrid waves with a relatively large range of k_{ES} have been performed using the Siple Station VLF transmitter in Antartica. Figure 20a shows typical data from these experiments in the form of a spectrogram of a 5.5-s, sweep-frequency pulse from the Siple Station VLF transmitter as received on the ISIS 2 spacecraft at 1400 km altitude above the station. The plasma parameters at the satellite at this time were roughly those indicated in Figure 8c. Lower hybrid waves were stimulated at each frequency of the pulse as the frequency swept from 6 to 4 kHz. According to our theory, this range of input wave frequency would produce lower hybrid wavelengths in the range 14 to 30 m. Figure 20b shows the amplitude of the pulse as a function of the calculated lower hybrid wavelength.

We propose to use the data of Figure 20b to demonstrate our method of determining $N(x)$ when E_x^{ES} is known over a significant range of k_x^{ES}. However, a few caveats are in order here. First of all, the data of Figure 20b, as well as all similar data, did not exhibit the typical fading characteristics associated with lower hybrid waves whose wave normals are limited to a narrow range of azimuths about $\mathbf{B}_0$ [*James and Bell*, 1987]. Instead, the distribution of wave normals about $\mathbf{B}_0$ appeared to be roughly isotropic, indicative of a two-dimensional scattering regime. Furthermore, since λ_{ES} is much smaller than the 75 m length of the ISIS 2 dipole antenna, the amplitudes shown in Figure 20b do not represent the true amplitudes of these waves. For instance, Gallagher's model [*Gallagher*, 1985] suggests a decrease in antenna sensitivity of roughly 20 dB for $\lambda_{ES} \sim 30$ m. Despite these deficiencies, it is instructive to use the data as it

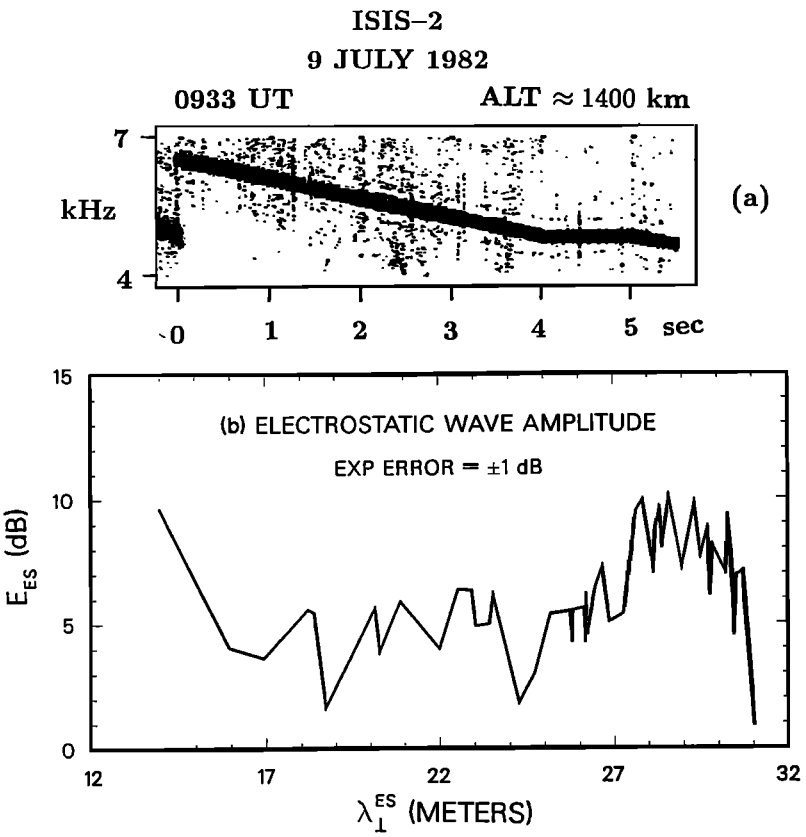

Fig. 20. (*a*) Spectrogram showing stimulated lower hybrid waves observed on the ISIS 2 satellite with total apparent bandwidth of approximately 300 Hz. (*b*) Measured amplitude of stimulated lower hybrid waves as a function of stimulated lower hybrid wavelength λ_{ES}.

stands to demonstrate how such data can be used to determine an apparent structure for the irregularities.

The calculation is as follows. According to (A8) , each major peak in the amplitude plot of Figure 20*b* indicates the presence of a Fourier component of $N(x)$ with approximately the same wavelength. The amplitude of each component ΔN_j can be estimated using (A8) and a trial value of W. This calculation provides a set of values of ΔN_j through which a trial density function, $\Delta N_t(x)$, can be constructed

$$\Delta N_t(x) \cong N_0 + \sum_j \Delta N_j e^{-ik_j x} \qquad (34)$$

where the sum is over the finite trial set.

Using (34) the following iterative process can be followed to determine $N(x)$:

1. The distribution of (34) is used in the simulation program described in section 2. The interval $0 \leq x \leq W$ is divided into 2000 planar slabs and the density in each slab is assumed to follow (34). The value of W is assumed to be no larger than 2 km, giving a slab width of no more than 1 m. The values of E_x^{ES} near $x \sim W/2$ are then plotted as a function of the wavelength of the lower hybrid waves.

2. The calculated values of E_x^{ES} are compared with the experimental values and the values of ΔN_j are adjusted accordingly, making use of the linear relationship between the excited lower hybrid field and ΔN_j.

3. The widths of the calculated peaks in E_x^{ES} are adjusted by varying W (see A9) so the bandwidth, Δk, of the calculated and observed peaks are similar.

4. Steps 1, 2, and 3 are repeated until good agreement is obtained between theory and observation.

The above procedure was used to determine a density distribution which could give rise to the observed lower hybrid wave spectrum. The magnitude of the coefficients ΔN_j for this distribution are plotted in Figure 21*b* and the predicted values of E_x^{ES}/E_x^{INC} are plotted in the dashed curve of Figure 21*a*. Also plotted are the observed values of the lower hybrid field increased by 18 dB to account for the decrease in antenna response at short wavelengths. It can be seen that reasonable agreement exists between theory and observation.

The above calculational procedure was used to derive a spatial structure for the irregularities which produced the data shown in Figure 20*a*. The total width W of the irregularity density distribution was determined to be approximately 1000 m. It can be seen that the dominant Fourier components in the irregularity density enhancement spectrum lie at $\lambda_x^{ES} \approx \lambda^{ES} \sim 30$ m.

5. DISCUSSION

The foregoing development has demonstrated that quasi-electrostatic lower hybrid waves of significant amplitude can be stimulated by electromagnetic whistler mode waves which scatter from planar magnetic-field-aligned plasma density irregularities in the top side ionosphere and magnetosphere. Below we discuss additional features of our model.

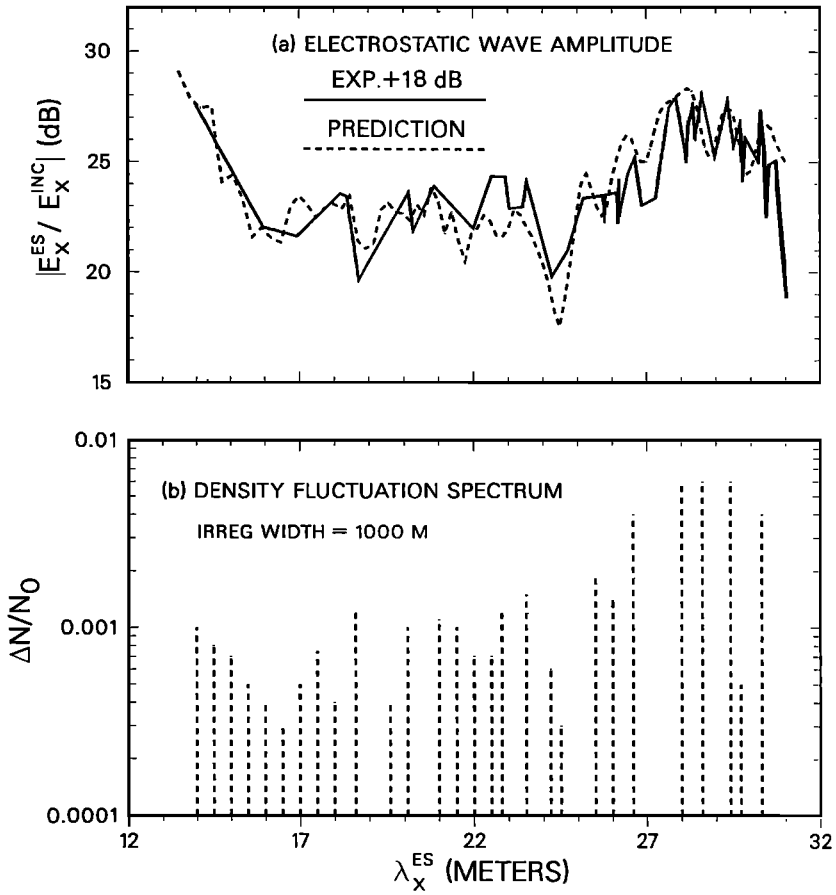

Fig. 21. (*a*) Theoretical prediction and measurement of stimulated lower hybrid wave amplitude. Experimental curve was raised by 18 dB to compensate for antenna response at short wavelengths. (*b*) Theoretical prediction of density fluctuation spectrum.

Coulomb Collisions

In the top side ionosphere Coulomb collisions between electrons and ions can play an important part in determining the propagation characteristics of the stimulated lower hybrid waves. To estimate the effects of these collisions we use the lower hybrid approximation for the dispersion relation of (9), i.e.,

$$k_x^{ES} = \pm k_{zi} \tan \psi_r = \pm k_{zi}(-P/S)^{1/2} \tag{35}$$

where ψ_r is the resonance cone half-angle. In the case of collisional energy losses, the parameters P and S will be complex numbers and the lower hybrid wave amplitude will decay along the x axis according to the relationship

$$\left|E^{ES}\right| \sim e^{-\alpha k_{zi}|x|} \tag{36}$$

where $\alpha = \text{Im}\,(-P/S)^{1/2}$.

Although α may be a large number in some cases, this does not necessarily mean that the lower hybrid waves will experience heavy damping, because the group velocity of the lower hybrid waves in the x direction is generally very small. In fact, if the effective Coulomb collision frequency ν is small compared to the wave frequency, the group velocity of the lower hybrid waves is perpendicular to the resonance cone half angle and we can write for the wave packet position,

$$\frac{dx}{dz} \cong \text{Re}\left[\frac{S}{-P}\right]^{1/2} \tag{37}$$

With the aid of (37) we can rewrite (36) as

$$\left|E^{ES}\right| \sim e^{-\beta k_{zi}|z|} \tag{38}$$

where $\beta = \text{Re}\,(-S/P)^{1/2} \times \text{Im}\,(-P/S)^{1/2}$. Considering only electron collisions we have

$$\begin{aligned} P &\cong \frac{-\omega_{0e}^2}{\omega(\omega - i\nu)} \\ S &\cong 1 + \frac{\omega_{0e}^2}{\omega_{He}^2}\left(1 + \frac{\nu}{i\omega}\right) - \frac{\omega_{0i}^2}{\omega^2} \end{aligned} \tag{39}$$

Assuming $\omega \gg \nu$, we can write

$$\beta \cong \frac{\nu}{2\omega} \cdot \frac{(2+\epsilon)(1+\epsilon)^{-1}\omega^2 - \omega_{LHR}^2}{(\omega^2 - \omega_{LHR}^2)} \tag{40}$$

where $\epsilon \equiv \omega_{He}^2/\omega_{0e}^2$.

The electron-ion collision frequency is described by the relation [*Rishbeth and Garriott*, 1969]

$$\nu = N\left[34 + 4.2\log_{10}(T^3/N)\right]T^{-3/2}$$

where N is the cold plasma density in c.g.s. units and T is the electron temperature.

At 300 km altitude we have $N \sim 10^5$ cm^{-3}, and $T \sim 1500^\circ$ K, for which $\nu \sim 91$, $f_0 \sim 3$ MHz, and $f_{He} \sim 1$ MHz. In this case for an input wave frequency of 10 kHz we find from (40)

$$\beta \cong 1.7 \times 10^{-3} \tag{41}$$

Although the stimulated lower hybrid wave amplitude can initially exceed that of the input wave, the waves will be difficult to detect experimentally if collisional damping causes their amplitude to decrease by more than 20 dB while propagating along $\mathbf{B}_0$. This limit implies a maximum propagation distance of $\Delta z \cong 2.3(\lambda_z/2\pi\beta)$, where λ_z is the wavelength along $\mathbf{B}_0$. Using (41) we find

$$\Delta z \sim 220\lambda_z \tag{42}$$

Since $\lambda_z \sim 1$ km, $\Delta z \sim 370$ km. However, the scale height for the cold plasma density at 300 km altitude is generally only 200 km. Thus the total attenuation for lower hybrid waves propagating toward higher altitudes from 300-km will be only ~ 10 dB. During daytime conditions, however, $N \sim 5 \times 10^5$ and if the electron temperature is the same, we find $\nu \cong 431$ and $\beta \cong 7.9 \times 10^{-3}$ and

$$\Delta z \sim 47\lambda_z \sim 47 \text{ km} \tag{43}$$

Consequently, lower hybrid waves stimulated near 300 km altitude during the daytime would probably not be observable at altitudes above 400 km.

We conclude that Coulomb collisions are not generally an important factor in the propagation of stimulated lower hybrid waves in the night time top side ionosphere. However, in the daytime, it appears that the stimulated lower hybrid waves will be significantly damped by Coulomb collisions in the altitude range 300–500 km.

Finite Temperature Effects

The properties of the stimulated lower hybrid waves will be modified by the effects produced by a finite temperature in the magnetoplasma. First of all, the maximum value of k_x for the stimulated waves will be limited by finite ion Larmor radius effects. Second, the waves may be damped through Landau and cyclotron resonance interactions with the thermal plasma components. The effects of finite ion Larmor radius can be neglected as long as k_x^{ES} obeys the following relation [*Stix*, 1962]:

$$\left(k_x^{ES}\right)^2 r_L^2 \ll 1 \tag{44}$$

where $r_L = (\kappa T_\perp/m_i)^{1/2}/\omega_{Hi}$ is the ion Larmor radius and where $T_\perp$ is the ion temperature in the plane perpendicular to $\mathbf{B}_0$, and κ is Boltzmann's constant. At 1400 km altitude at mid-latitude with $T_\perp \sim 1500^\circ$ K, (44) yields for H^+ ions

$$\left(\lambda_x^{ES}\right)^2 \gg (8 \text{ m})^2 \tag{45}$$

A similar calculation for altitudes near the magnetic equatorial plane at $L \sim 2.0$ yields the restriction

$$\left(\lambda_x^{ES}\right)^2 \gg (64 \text{ m})^2 \tag{46}$$

Given that (44) is satisfied, the dispersion relation for quasi-electrostatic waves can be written (*Stix*, [1962] Chapter 9)

$$k_x^2 S + k_z^2 P + i\pi^{1/2}\alpha\omega_{0e}^2 v_T^{-2} e^{-\alpha^2} = 0 \tag{47}$$

where v_T is the rms thermal velocity of the electrons, $\alpha = |\omega/k_z|(m_e/2\kappa T_\parallel)^{1/2}$, and where we have assumed that the electrons and ions have maxwellian thermal velocity distributions of equal temperatures and that $\alpha^2 \gg 1$. In (47) we include only Landau damping, since cyclotron damping is negligible when $\omega \ll \omega_{He}$.

In the case of planar irregularities which are strictly parallel to $\mathbf{B}_0$, by Snell's law, $k_z^{ES} = k_z^i$, and $\omega/k_z^{ES} \gg v_T$, and $\alpha_0^2 \gg 1$. Thus Landau damping is negligible in (47) .

When the planar irregularity is not strictly parallel to $\mathbf{B}_0$, Landau damping may be significant. To see this we note that (47) applies to a system in which $\mathbf{B}_0$ is parallel to the z axis. Any solution of (47) for a given value of n_{zi} can be expressed in the first system by the coordinate transformation

$$\begin{aligned} n_x' &= n_x \cos\chi + n_{zi} \sin\chi \\ n_z' &= n_{zi} \cos\chi - n_x \sin\chi \end{aligned} \tag{48}$$

where the primed variables apply to the system in which $\mathbf{B}_0$ is parallel to the z axis, and n_x is a solution of (47) . Now if $|\chi| \to \chi_c$, then for one of the lower hybrid waves, $n_x \to \infty$. In this case (48) shows that $n_z' \to \infty$, also. Thus the phase velocity of the wave along $\mathbf{B}_0$ will decrease and Landau damping will increase accordingly, as indicated in (47) .

Making use of (37) and (47) , the amplitude change due to Landau damping can be written in the form shown in (38) where now

$$\beta \cong \sqrt{\pi}\alpha^3 e^{-\alpha^2} \tag{49}$$

Experimental results [*Bell et al.*, 1983] suggest that the lower hybrid waves can propagate over distances at least of the order of 10^3 km, or roughly 10^3 wavelengths along $\mathbf{B}_0$. Lower hybrid waves which are damped more than 20 dB over this distance would be difficult to observe. A 20-dB maximum damping loss over 10^3 wavelengths implies $\beta \sim 4 \times 10^{-4}$, a value for which (49) yields $\alpha \sim 3.5$.

Making use of the definition of α and assuming an electron temperature of 1500° K, we then obtain

$$n_{zi} \leq 4 \times 10^2 \tag{50}$$

Combining (35), (39), and (50), we obtain

$$\left|k_x^{ES}\right| \leq 4 \times 10^2 \frac{\omega_{He}}{c}\left[(1+\epsilon)(1-\omega_{LHR}^2/\omega^2)\right]^{-1/2} \tag{51}$$

where ϵ is defined in (40).

At 1400 km altitude at mid-latitude we have $f_{He} \sim 880$ kHz and $\epsilon \sim 0.2$, and finding λ_{ES} from (51), we have

$$\lambda_{ES} > (1 - \omega_{LHR}^2/\omega^2)^{1/2} \text{ m}. \tag{52}$$

Similarly, at $L \sim 2$ near the magnetic equatorial plane where $f_{He} \sim 110$ kHz, we obtain

$$\lambda_{ES} > 8(1 - \omega_{LHR}^2/\omega^2)^{1/2} \text{ m} \tag{53}$$

Since (52) and (53) are much weaker constraints than (45) and (46), we conclude that Landau damping by the main thermal plasma component will not be significant for the lower hybrid waves considered in the present study. However, if the electron velocity distribution contains a significant high energy tail in addition to the Maxwellian component, this conclusion would need to be reexamined.

Experimental data indicate that the maximum Doppler shift in 10- to 14-kHz signals observable at 1400 km at mid-latitudes is approximately $|\Delta f_D| \sim 500$ Hz. Using the

Doppler shift relation $\Delta f_D = \mathbf{k} \cdot \mathbf{v}_s/2\pi$ and a typical satellite velocity v_s of ~ 7 km/s we can find the wavelength of the observed lower hybrid wave

$$\lambda^{ES} \sim 7 \text{ km/s}/500 \text{ Hz} \sim 14 \text{ m} \tag{54}$$

where we have assumed that the angle between $\mathbf{v}_s$ and $\mathbf{k}$ is small. Experimental data [*Bell and Ngo*, 1988] also indicate that the maximum Doppler shift in 10 to 14 kHz signals observable at $L \sim 2$ near the magnetic equatorial plane is $|\Delta f_D| \sim 50$ Hz. With a satellite velocity of 5 km/s this implies a wavelength of

$$\lambda^{ES} \sim 5 \text{ km/s}/50 \text{ Hz} \sim 100 \text{ m} \tag{55}$$

where again we have assumed that $\mathbf{v}_s$ and $\mathbf{k}$ are roughly parallel.

Note that the wavelength values given in (54) and (55) satisfy the restriction stated in (45) and (46). Thus we conclude that the zero temperature approximation used in the present work should apply to the major portion of the observational data.

Comparison With Past Work

In a general sense our work can be viewed as a contribution to the study of electromagnetic wave propagation in an inhomogeneous magnetoplasma. This topic has received much study over the past few decades, and a thorough review of early work on this subject can be found in *Budden* [1985]. In particular, the early work of *Clemmow and Heading* [1954] and *Försterling* [1942] are relevant to our work in that their coupled wave equations indicate in general, the conditions under which strong mode coupling effects can be expected between the four possible normal modes. However, neither work explicitly considers the question of irregularities or the excitation of quasi-electrostatic waves. Apparently, the first work concerning the propagation of electromagnetic waves in a magnetoplasma in the presence of irregularities was carried out by *Budden* [1961] and *Simonich and Yeh* [1972], but this work did not deal with the excitation of quasi-electrostatic waves. Somewhat later a number of papers concerning the propagation of whistler mode waves within magnetic-field-aligned plasma density irregularities known as whistler mode ducts, discussed the mode coupling that occurs because of the plasma density variation across the duct [*Northover*, 1959*a*, *b*; *Adachi*, 1965; *Scarabucci and Smith*, 1971]. However, these papers did not explicitly consider the excitation of quasi-electrostatic waves. More recently, *Antani and Kaup* [1984] using a perturbation theory have dealt with the problem of whistler mode waves scattering from random fluctuations in a magnetoplasma and have derived an expression for the dispersion relationship for the electromagnetic whistler mode waves. This dispersion relationship contains an effective damping coefficient which accounts for the wave energy scattered into the quasi-electrostatic modes. The authors assume the fluctuations in the plasma are caused by drift-wave type turbulence with a scale of the ion gyroradius. No direct comparison of this work with our own can be made since the authors did not calculate the amplitude of the excited lower hybrid waves.

Other aspects of the transformation of electromagnetic to electrostatic wave energy through linear mode coupling have been considered recently in other fields. For example, *Wong et al.* [1981] have discussed the direct conversion of electromagnetic HF waves into electrostatic Langmuir waves in the ionosphere during heating experiments, and *Morales et al.* [1985] have discussed the direct conversion of fast Alfven waves into ion Bernstein modes in Tokamak devices. Thus there is evidence that linear mode conversion can be an important process over a wide range of plasma and wave parameters.

Alternative theories to explain the excitation of lower hybrid waves by electromagnetic whistler mode waves have been advanced by *Titova et al.* [1984] and *Groves et al.* [1988]. The mechanism of Titova et al. involves nonlinear resonance scattering and assumes that the input electromagnetic waves are scattered by plasma density irregularities associated with ion acoustic turbulence. The ion acoustic waves are hypothesized to be produced through the action of magnetic-field-aligned electric currents. While ion acoustic turbulence and field-aligned electric currents are common at high latitude, there is little evidence to suggest that they also occur at mid-latitudes, a region where lower hybrid wave stimulation is often observed. Furthermore, there is no evidence that ion acoustic turbulence is commonly present within the inner radiation belt, another region where lower hybrid wave stimulation is commonly observed. This discrepancy raises serious question concerning the applicability of the Titova et al. mechanism.

Groves et al. [1988] have proposed two different mechanisms which they think may be involved in the lower hybrid wave stimulation. The first mechanism involves nonlinear wave scattering by preexisting one-dimensional magnetic-field-aligned plasma density irregularities with sinusoidal variation perpendicular to $\mathbf{B}_0$. It is assumed that the input electromagnetic wave is propagating strictly parallel to $\mathbf{B}_0$. In this case the normalized amplitude of the excited lower hybrid wave has the value $E_x^{ES}/E_x^{INC} = \Delta N/N_0$. Thus for small ΔN the predicted amplitude of the nonlinearly generated lower hybrid wave is generally orders of magnitude smaller than the values our passive linear scattering model predicts. Consequently, we conclude that the nonlinear wave scattering mechanism of Groves et al. is too weak to explain the observed data.

The second mechanism advanced by Groves et al. involves a parametric excitation of short wavelength lower hybrid waves by electromagnetic whistler mode waves. This four wave interaction mechanism takes place only if the input wave amplitude exceeds a threshold level E_m which the authors calculate to be $E_m \sim 18$ mV/m at low altitudes. There are at least two difficulties with this mechanism. First of all the parametrically excited lower hybrid waves take a relatively long time to develop, as much as a few seconds after the VLF input wave arrives in the generation region [*Lee and Kuo*, 1984]. On the other hand observations indicate that the lower hybrid waves are commonly excited within 50 ms of the arrival of the input wave [*Bell et al.*, 1983; *Bell and Ngo*, 1988]. Another difficulty lies in the prediction of the wavelength of the excited lower hybrid waves. Groves et al. state that the parametric instability will preferentially excite lower hybrid waves with a wavelength $\lambda \sim 90$ m at the satellite location. For a satellite velocity of 7 km/s this gives a Doppler shift of roughly 80 Hz for the lower hybrid waves. On the other hand, commonly observed Doppler shifts of excited lower hybrid waves are as large as 500 Hz at low altitude ($\sim$ 1000) km [*Bell et al.*, 1983]. Thus there appears to be a significant discrepancy between the prediction of the Groves et al. model and the observations.

Effective Wave Damping Through Mode Coupling

At each irregularity, some of the energy of the incident electromagnetic whistler mode wave will be transformed into lower hybrid wave energy. This situation results in an effective damping of the electromagnetic whistler mode wave [*Antani and Kaup*, 1984]. To see this, consider the case in which the irregularities are substantially identical. Since the Poynting flux is conserved along the x axis, we can write

$$\Delta P_x^{WM} = -\eta P_x^{ES} \Delta x \tag{56}$$

where ΔP_x^{WM} is the change in the total electromagnetic energy flux in the x direction, P_x^{ES} is the total electrostatic energy flux excited at each irregularity, η is the number of irregularities per unit length along the x axis, and where it is assumed that the irregularities are randomly spaced along the x axis with an average spacing larger than λ_{ES}. Since at any given irregularity we can use the boundary conditions on $\mathbf{E}$ and $\mathbf{B}$ to find the ratio $\alpha = P_x^{ES}/P_x^{WM}$, we can write (56) in the form

$$\Delta P_x^{WM} = -\alpha\eta P_x^{WM} \Delta x \tag{57}$$

In the limit of small Δx, (57) can be integrated to yield

$$P_x^{WM} \cong P_{x0}^{WM} e^{-\alpha\eta x} \tag{58}$$

where P_{x0}^{WM} is the energy flux originally incident on the irregularity region. From (58) it can be seen that the electromagnetic whistler mode wave would suffer a 4.5 dB loss over the distance

$$x_d \sim (\alpha\eta)^{-1} \tag{59}$$

Since the group velocity of the electromagnetic whistler mode wave is principally along $\mathbf{B}_0$, it is useful to express (59) in terms of the total propagation distance along this direction

$$z_d \sim (\alpha\eta)^{-1} V_{Gz}/V_{Gx} \tag{60}$$

where z_d is the distance the electromagnetic wave propagates along $\mathbf{B}_0$ while traversing the distance x_d through the irregularity region, and where V_{Gx} and V_{Gz} are the components of the group velocity vector along the x and z axes, respectively. For small values of wave normal angle θ it can be shown that

$$z_d \sim 2(\alpha\eta\theta)^{-1} \tag{61}$$

For $f = 15$ kHz numerical values for z_d can be obtained with the use of Figure 22. Figure 22*a* shows the Poynting flux (P_x) distribution among the four characteristic modes when the input electromagnetic whistler mode wave encounters an irregularity of Gaussian cross section identical to that shown in Figure 15, but with arbitrary density enhancement $\Delta N/N_0$. It can be seen that for $\Delta N/N_0 \leq 20\%$ the energy of the reflected electromagnetic whistler mode wave is negligible compared to that of the two lower hybrid modes, which carry equal energy in opposite directions.

As an example consider the case where $\Delta N/N_0 \sim 2\%$ and $\eta \sim 2$ km^{-1}. According to Figure 22, $\alpha \sim 10^{-3}$, and thus $z_d \sim 3000$ km for this case. Stronger damping of the electromagnetic whistler mode wave will occur if the irregularity density perturbation is larger than 2%. For instance, when $\Delta N/N_0 \sim 5\%$ and all other parameters are the same, it is found that $z_d \sim 1000$ km.

These two cases illustrate the fact that the presence of small scale magnetic-field-aligned density irregularities

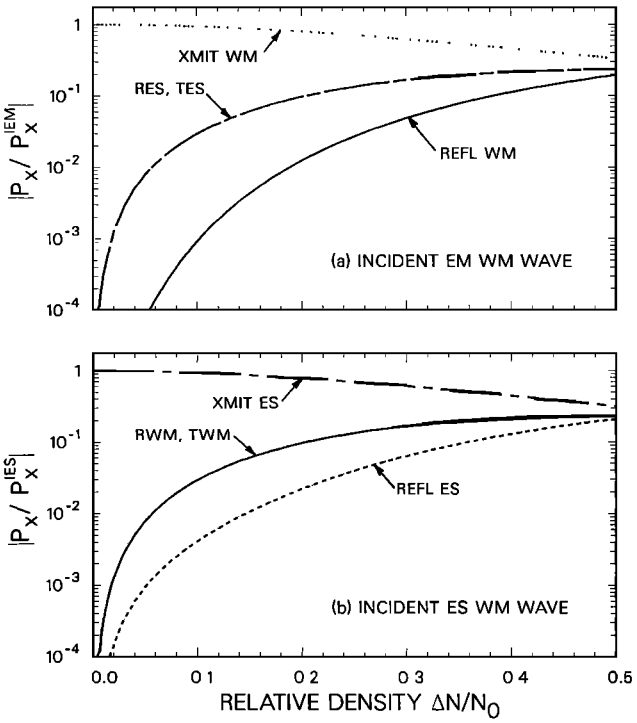

Fig. 22. (*a*) Normalized Poynting flux P_x/P_x^{IEM} of the four characteristic waves excited as an input electromagnetic whistler mode wave encounters a magnetic-field-aligned Gaussian density enhancement. (*b*) Normalized Poynting flux P_x/P_x^{IES} of the four characteristic waves excited as an input quasi-electrostatic whistler mode wave (lower hybrid wave) encounters a magnetic-field-aligned Gaussian density enhancement.

can lead to significant damping of electromagnetic whistler mode waves which propagate through the irregularity region. This type of damping may be the most important damping mechanism for electromagnetic whistler mode waves throughout large regions of the magnetosphere where small scale magnetic-field-aligned plasma density irregularities are known to exist [*Bell and Ngo*, 1988; *Fejer and Kelley*, 1980].

Once they are excited, lower hybrid waves will also lose energy to the other characteristic modes through mode coupling. Figure 22*b* shows the Poynting flux distribution among the four characteristic modes when an input lower hybrid wave encounters a Gaussian irregularity identical to that shown in Figure 15, but with arbitrary density enhancement. It can be seen that the input wave loses energy mainly to the two excited electromagnetic whistler mode waves, which carry equal energy in opposite directions. Values of z_d for the lower hybrid waves are also given by (60), but the ratio of group velocity components is much larger for these waves because their group velocity vector is perpendicular to the whistler mode resonance cone. Thus for the lower hybrid waves we have

$$z_d \sim (\alpha\eta\chi_c)^{-1} \tag{62}$$

For $f = 15$ kHz, $\chi_c \sim 1^\circ$ and thus it is found that the lower hybrid waves can propagate roughly 5 times as far as the electromagnetic waves before losing significant energy through mode coupling.

In the above arguments it is important to remember that in general, the amplitude of the excited lower hybrid waves depends upon the width of the irregularity as well as the

peak density enhancement. For instance, it can be deduced from Figure 16 that a Gaussian irregularity of 5% enhancement and 14 m half-width produces 10 dB less lower hybrid wave energy than a similar Gaussian enhancement of 4 m half-width. Thus the effective propagation distance of an electromagnetic whistler mode wave in a region of irregularities will show a first-order dependence upon the width of the irregularities.

Suggestions for Future Work

A definitive test of the theory of lower hybrid wave stimulation proposed in the present paper requires high resolution comprehensive satellite measurements of the **E** and **B** fields of the stimulated waves, as well as the density of the local plasma. Three orthogonal axes measurements of the **E** field of the stimulated waves need to be made to establish the direction of **E** and its orientation with respect to the static magnetic field $\mathbf{B}_0$ and the whistler mode resonance cone. Three-axis high sensitivity measurements of the small **B** field of the quasi-electrostatic lower hybrid waves are needed to establish the magnitude and direction of **B**, the direction of the Poynting flux $\mathbf{E} \times \mathbf{H}^*$, and the values of various characteristic polarization ratios (e.g., E_x/H_y) which can be used to identify plasma waves.

Simultaneous high resolution measurements of the local plasma density are needed to determine the irregularity structure within which the lower hybrid waves are stimulated. Since the velocity of low altitude satellites ranges from 5 to 7 km/s, plasma density measurements would need to be repeated at a rate of 1 kHz to achieve a resolution of roughly 5 m. This rate is well within the capabilities of present day Langmuir probes. The three-axis, orthogonal dipole antennas used to detect the **E** field of the lower hybrid waves should be as short as possible so that the effective length of the antennas will be the same for all wavelengths detected. A tip-to-tip length of 5 to 10 m would satisfy this requirement in general and would still provide a reasonable S/N ratio in most cases.

The possible association of the stimulated lower hybrid waves with energetic electron precipitation [*Bell et al.*, 1983] could be determined using energetic particle detectors covering the range 100 eV to 100 keV.

Although the measurements suggested above can be made using input signals from existing VLF transmitters, their formats are not generally ideal. As a better input signal we suggest a set of 50-ms pulses separated by 1 kHz and transmitted simultaneously in a "comb" format, as shown in Figure 23*a*. The frequency range of these pulses would extend from a few kHz below f_{LHR} up to roughly $10 f_{LHR}$. Each input pulse would excite lower hybrid waves whose wavelength was a function of the input pulse frequency, as indicated schematically in Figure 23*b*. With 1-kHz separation between pulses, Doppler shifts of up to ±500 Hz in the stimulated waves could be accommodated without overlap of lower hybrid waves stimulated by adjacent pulses. The comb pulse format could be repeated every 100 ms to yield a spatial resolution of roughly 500 m along the satellite path. A series of short input pulses is superior to a CW signal since a measure of the time delay between each pulse and its associated lower hybrid waves is necessary to determine the range to the scattering region. The frequency resolution of the comb format could be improved at the expense of the temporal (spatial) resolution. For instance, each pulse in the comb format could be shifted in frequency by an amount $\Delta f = s^{-1}$ kHz, where s is a positive integer, each time a comb group was transmitted. Each sth comb group would then be the same. To avoid overlap between lower hybrid waves stimulated by one pulse group and the input pulse from the next comb group, the time $\Delta\tau$ between successive comb groups would have to be increased to as much as 250 ms. If $\Delta f = 250$ Hz and $\Delta\tau \sim 250$ ms, a spatial resolution of roughly 1 km could be achieved. A 1-km resolution along the satellite path may be adequate since the cross-L scale of the irregularity region which contributes to the lower hybrid wave field at the satellite appears to be roughly of the same magnitude.

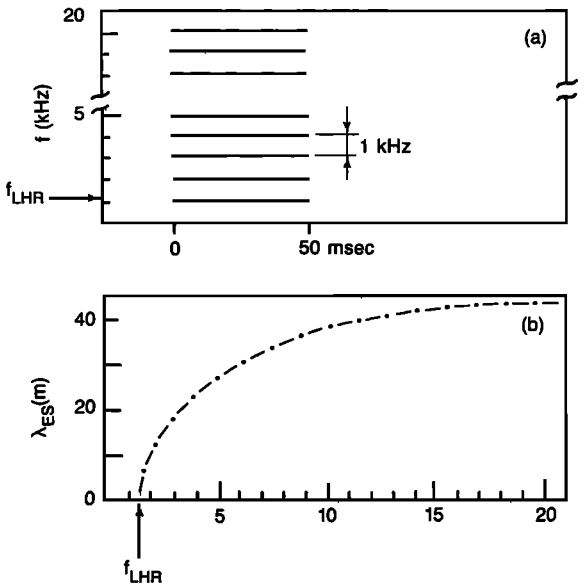

Fig. 23. (*a*) Proposed format of transmission of VLF signals used to detect small scale magnetic-field-aligned plasma density irregularities in the ionosphere and magnetosphere. (*b*) Wavelengths of lower hybrid waves excited by input signals.

The wave measurements described above would allow the complete characterization of the **E** and **B** fields of the lower hybrid waves and their variation as a function of input wave frequency. On the other hand, the local plasma density measurements will not determine whether the measured irregularities are magnetic-field-aligned or planar in nature. However, this determination could in principal be made by a multisatellite group, such as that planned for the Cluster Mission.

6. SUMMARY

We have demonstrated that high amplitude, short wavelength (5 m $\leq \lambda \leq$ 100 m) quasi-electrostatic whistler mode waves can be excited when electromagnetic whistler mode waves scatter from small-scale planar magnetic-field-aligned plasma density irregularities in the topside ionosphere and magnetopshere. These waves cut off at the lower hybrid resonance frequency and are a type of lower hybrid wave. The mechanism of excitation involves linear mode coupling between the four characteristic modes of the cold magne-

tosplasma in regions of changing plasma density. Our model predicts the following behavior:

1. Lower hybrid waves are strongly excited only when the scale of the electron density irregularity is of the order of the wavelength of the lower hybrid wave (5–100 m).

2. Lower hybrid waves are strongly excited only when the planar electron density irregularities are aligned within a few degrees of $\mathbf{B}_0$.

3. Electromagnetic whistler mode waves can experience significant effective damping as the lower hybrid waves are excited. This form of damping may be the most important damping mechanism for whistler mode waves throughout large regions of the magnetosphere.

4. Through a VLF "radar" technique the electrostatic wave spectrum can be used as a diagnostic tool to determine the structure of small scale irregularities in the magnetosphere.

APPENDIX

From (6) and (12) we can express the divergence of $\mathbf{D}$ in the form

$$\frac{\partial}{\partial x}[SE_x] - ik_z PE_z = i\frac{\partial}{\partial x}(DE_y) \tag{A1}$$

where we have assumed $k_y \cong 0$.

In the limit as $k_x^{ES} \to \infty$, the components of the electrostatic field can be derived from a scalar potential function $\Phi(x)$, where

$$\begin{aligned} E_x^{ES} &= -\frac{\partial \Phi(x)}{\partial x} \\ E_z^{ES} &= ik_z \Phi(x) \end{aligned} \tag{A2}$$

In the limit of weak scattering where $(\Delta N/N)^2 \ll 1$, the electromagnetic components of (A1) can be approximated by the input wave fields. In these two limits (A1) can be rewritten

$$\frac{\partial}{\partial x}\left[S\frac{\partial \Phi(x)}{\partial x}\right] + Sk^2\Phi(x) = iE_y^{INC}\frac{\partial D}{\partial x}\exp(-ik_x^{INC}x) \tag{A3}$$

where now $k \equiv k_x^{ES} = k_z|P/S|^{1/2}$. In (A3) the parameters S and D are defined as in (8), and it is assumed that neither of them vary significantly over a distance comparable to λ^{ES}.

We now express the electron density as a Fourier series over the interval $0 \le x \le W$, the region of space assumed to contain the irregularities

$$N(x) = N_0 + \sum_{m=-\infty}^{\infty} \Delta N_m e^{-ik_m x} \tag{A4}$$

where $k_m = 2\pi m/W$, and N_0 is the background density. Substituting (A4) into (A3), making use of the definition of D and neglecting terms of order $(\Delta N(x)/N_0)^2$, we can find the following expression for E_x^{ES}

$$\frac{E_x^{ES}(x)}{E_x^{INC}} = \rho_y \frac{D_0}{S_0} \sum_{m=-\infty}^{\infty} k_m \frac{\Delta N_m}{N_0} G(k, k', x) \tag{A5}$$

where D_0 and S_0 are evaluated for $N(x) = N_0$, $k' \equiv k_m + k_x^{INC}$, where ρ_y is defined in (14), and where

$$\begin{aligned} G(k, k', x) = i(k^2 - k'^2)^{-1}\Big[&k'e^{-ik'x} \\ &- \tfrac{1}{2}(k + k')e^{i(k-k')W}e^{-ikx} + \tfrac{1}{2}(k - k')e^{ikx}\Big] \end{aligned} \tag{A6}$$

The term $G(k, k', x)$ in (A6) has a maximum value when $k \equiv k_x^{ES} = \pm(k_m + k_x^{INC})$. Since $k_x^{ES} \gg k_x^{INC}$, this corresponds to the condition in which the lower hybrid waves excited in the irregularity structure possess a wavelength closely equal to the wavelength of one of the spatial Fourier components of the irregularity density distribution. In this case the waves add coherently along the x direction. This type of behavior is illustrated in Figure 17.

When $k \to \pm k'$, the leading term of (A5) can be written

$$G(k, k') \underset{k \to k'}{\cong} -\tfrac{1}{2}i(W - x)e^{i(W-x)k'} \tag{A7a}$$

$$G(k, k') \underset{k \to -k'}{\cong} \tfrac{1}{2}ixe^{ik'x} \tag{A7b}$$

Thus if the observation point is near the midpoint of the irregularity system and $k \to k_j$ where k_j is one of the k_m, the leading term of the expression for E_x^{ES} has the value

$$\begin{aligned} E_x^{ES} \underset{k \to k_j}{\cong} &\tfrac{1}{4}k_j W E_x^{INC} D_0 S_0^{-1} N_0^{-1} \\ &\times \left[\Delta N_j e^{ik_j x} - \Delta N_j^* e^{ik_j(W-x)}\right] \end{aligned} \tag{A8}$$

where ΔN_j^* is the complex conjugate of ΔN_j, $x \sim W/2$, and where we have made use of the fact that $E_y^{INC} \cong iE_x^{INC}$. Thus E_x^{ES} is linearly proportional to the product $k_j W$, which represents the number of electrostatic wavelengths contained in the irregularity region.

Assuming that $k_j W \gg 1$, the value represented by (A8) can be attained only over a narrow range of wave numbers, Δk, centered on k_j, where

$$\Delta k \sim W^{-1} \tag{A9}$$

Acknowledgments. We wish to acknowledge the many valuable discussions we have held with our colleagues in the STAR Laboratory during the course of this work. The manuscript was prepared by G. Walker. This research was sponsored by the National Aeronautics and Space Administration under contracts NGL-05-020-008, NAGW-1680, and NAGS-1103.

The Editor thanks D.L.Gallagher and another referee for their assistance in evaluating this paper.

REFERENCES

Adachi, S., Study on the guiding mechanism of whistler radio waves, *J. Res. Natl. Bur. Stand., Sect. D, 69*, 493, 1965.

Antani, S. N., and D. J. Kaup, Whistler scattering from density fluctuations in magnetized plasmas, *Phys. Fluids, 27,* 1169, 1984.

Bell, T. F., and H. D. Ngo, Electrostatic waves stimulated by coherent VLF signals propagating in and near the inner radiation belt, To be published in *J. Geophys. Res., 88,* 2599, 1988.

Bell, T. F., H. G. James, U. S. Inan, and J. P. Katsufrakis, The apparent spectral broadening of VLF transmitter signals during transionospheric propagation, *J. Geophys. Res., 88,* 4813, 1983.

Berger, R. L., and F. W. Perkins, Thresholds of parametric instabilities near the lower-hybrid frequency, *Phys. Fluids, 19,* 406, 1976.

Born, M., and E. Wolf, *Principles of Optics*, 3rd edition Pergamon, New York 1970.

Brekke, A., *Radar Probing of the Aurora Plasma, Proceedings of the EISCAT Summer School, Tromso, Norway, June 5–13, 1975*, Columbia University Press, New York, 1977.

Budden, K.G., *Radio waves in the ionosphere*, 1st edition, Cambridge University Press, London, 1961.

Budden, K. G., *The Propagation of Radio Waves*, Cambridge University Press, New York, 1985.

Clemmow, P. C., and J. Heading, Coupled forms of the differential equations governing radio propagation in the ionosphere, *Proc. Cambridge Phil. S., 50*, 319-333, 1954.

Fejer, B. G., and M. C. Kelley, Ionospheric irregularities, *Rev. Geophys., 18*, 401, 1980.

Försterling, K., Über die Ausbreitung elektromagnetischer Wellen in einem magnetisierten Medium bei senkrechter Incidenz, *Hochfrequenztech. Elektroakust., 59*, 10, 1942.

Gallagher, D. L.,, Short wavelength electrostatic waves in the Earth's magnetosheath, *J. Geophys. Res., 90,* 1435, 1985.

Groves, K. M., M. C. Lee, and S. P. Kuo, Spectral broadening of VLF radio signals traversing the ionosphere, *J. Geophys. Res., 93,* 14683, 1988.

Inan, U. S., and T. F. Bell, Spectral broadening of VLF transmitter signals observed on DE1: a quasi-electrostatic phenomenon?, *J. Geophys. Res., 90,* 1771, 1985.

James, H. G., and T. F. Bell, Spin modulation of spectrally broadened VLF signals, *J. Geophys. Res., 92,* 7560, 1987.

Lee, M. C., and S. P. Kuo, Production of lower hybrid waves and field-aligned plasma density striations by whistlers, *J. Geophys. Res., 89,* 10,873, 1984.

Morales, G. J., S. N. Antani, and B. D. Fried, Direct conversion of a fast wave into ion Bernstein modes caused by density fluctuations, *Phys. Fluids, 28*, 3302, 1985.

Northover, F. H., The propagation of electromagnetic waves in ionized gases with special reference to whistlers, *J. Atmos. Terr. Phys., 17*(1/2), 158, 1959*a*.

Northover, F. H., The propagation of electromagnetic waves in ionized gases, *IEEE Trans. Antennas Propag., AP-7, Suppl.*, S340, 1959*b*.

Ngo, H. D., and T. F. Bell, Quasi-electrostatic waves excited during the scattering of coherent whistler-mode waves from magnetic-field-aligned plasma density irregularities, *Eos Trans. AGU, 66*, 1038, 1985.

Rishbeth, H., and O. K. Garriott, *Introduction to Ionospheric Physics*, Academic, San Diego, Calif.,1969.

Scarabucci, R. R., and R. L. Smith, Study of magnetospheric field oriented irregularities – The mode theory of bell-shaped ducts, *Radio Sci., 6*, 65, 1971.

Semat, H., *Introduction to Atomic Physics,* Rinehartaud, New York, 1946.

Simonich, D. M., and K. C. Yeh, A theory of scattering from irregularities in a magneto-ionic medium, *Radio Sci., 7*, 291, 1972.

Stix, T. H., *The Theory of Plasma Waves,* McGraw-Hill, New York, 1962.

Tanaka, Y., M. Hayakawa, D. Lagoutte, and F. Lefeuvre, Study of the middle latitude broadening of the spectrum of the waves emitted from ground, Paper presented at International Conference on Results of the ARCAD-3 Project and of Recent Programmes in the Magnetospheric and Ionospheric Physics, Cent. Natl. d'Etud. Spatiales, Toulouse, France, May, 1984.

Titova, E. E., V. I. Di, V. E. Yurov, O. M. Raspopov, V. Yu Trakhtengertz, F. Jiricek, and P. Triska, Interaction between VLF waves and turbulent ionosphere, *Geophys. Res. Lett., 11,* 323, 1984.

Wong, A. Y., G. J. Morales, D. Eggleston, J. Santoru, and R. Behnke, Rapid conversion of electromagnetic to electrostatic waves in the ionosphere, *Phys. Rev. Lett., 47*, 1340, 1981.

T. F. Bell and H. D. Ngo, STAR Laboratory, Department of Electrical Engineering/SEL, Durand 315, Stanford University, Stanford, CA 94305.

(Received March 17, 1989;
revised June 2, 1989;
accepted June 8, 1989.)